Title
Engineering Adhesion Substrates as Biomaterials for Cell Fate Control

Author
Wong, Sze Yue

Publication Date
2016

Peer reviewed|Thesis/dissertation

Engineering Adhesion Substrates as Biomaterials for Cell Fate Control

By

Sze Yue Wong

A dissertation submitted in partial satisfaction of the

requirements for the degree of

Joint Doctor of Philosophy

with the University of California, San Francisco

in

Bioengineering

in the

Graduate Division

of the

University of California, Berkeley

Committee in charge:

Professor Song Li, Chair
Professor Tamara Alliston
Professor Lin He

Fall 2016

Engineering Adhesion Substrates as Biomaterials for Cell Fate Control

By

Sze Yue Wong

University of California, Berkeley

Abstract

Engineering Adhesion Substrates as Biomaterials for Cell Fate Control

By

Sze Yue Wong

Joint Doctor of Philosophy
with the University of California, San Francisco

in Bioengineering

University of California, Berkeley

Professor Song Li, Chair

The microenvironment is known to influence cell state and behavior. In turn, cells interact with and remodel their niches. A comprehensive understanding of this bidirectional interaction is crucial to guide our design of next-generation biomaterials so as to be able to accurately control cell fate in a precise and predictable manner. In Chapter 2 of this dissertation, we present for the first time a biphasic dependence of direct neuron reprogramming, the direct conversion of adult fibroblasts into neurons without passing through a pluripotent state, on adhesion substrate stiffness. We determined that this occurred through stiffness-regulation of cell signaling pathways and additionally observed this relationship to be time-dependent and limited to the early phases of direct reprogramming. Altogether, our results provide insights into the roles of substrate stiffness in regulating direct reprogramming and the underlying mechanism, which will open a new avenue for the rational design of smart biomaterials for direct cell reprogramming. In Chapter 3, we describe the isolation of native ECM proteins from human placentas and characterize these for potential *in vivo* tissue regeneration applications. Finally, in Chapter 4, we discuss the rationale for and the process of generation and characterization of a novel autologous acellular ECM scaffold for application in small diameter vascular graft replacement.

Dedicated to my family

Acknowledgements

I will like to thank the Agency for Science, Technology and Research, Singapore for funding my PhD at the University of California, Berkeley, without which this PhD journey would not have been possible.

Likewise, I will like to express my appreciation to my advisor Professor Song Li for his advice, optimism and encouragement in the last five years. I appreciate the opportunities that I have had in this lab. I have learnt much from my advisor in science and definitely even more beyond. I wish to acknowledge my qualifying exam committee – Gerard Marriott, Anthony Hunt, Xiaohua Gong and Shaofan Li and also my dissertation committee – Tamara Alliston and Lin He.

I am particularly grateful to colleagues who have co-authored the work in this dissertation. This work would not have been possible without the contribution of Jennifer Soto, Julia Chu, Hyungju Park and Douglas O Kelkhoff and Xuefeng Qiu. Thank you to all of you for so generously sharing your expertise and knowledge. In particular, I want to express my sincere gratitude to Julia Chu for all her help in my experiments and to Jennifer, Doug and Xuefeng for the time they have invested into finalizing our manuscripts for publication.

I will also like to express my heartfelt thanks to past and present Li lab members for their support in the last five years. I especially want to thank Jeff Henry for his guidance when I first joined the lab, Timothy Downing for sharing his experience and insights when we first started the neuron reprogramming project and Julia Chang for all the insightful discussions we had together. Thank you to fellow lab mates Julia Chu, Shyam Patel, Jeff Henry, Xuefeng Qiu, Timothy Downing, Helen Huang, Benjamin Lee, Julia Chang, Jennifer Soto, Wen-Chin Huang, Jaren Sia, Weixi Zhong, Douglas Kelkhoff, Zoey Huang, Tiffany Dai and Elaine Su for your scientific discussions, friendship and emotional support which made time in the lab fun. Each of you are unique and I have learnt so much, both in science and otherwise, from every single one of you. I also have to thank past undergrads in the Li lab – Surya Kotha, Kellen Chen and Vivian Shen who have worked with me and helped me in my projects.

Finally, thank you to my family for their support and encouragement. I am eternally grateful.

Table of Contents

Chapter 1: Introduction

1.1 Dissertation Introduction 1

1.2 Dissertation Outline 2

Chapter 2: Biophysical Regulation of Direct Cell Reprogramming and the Underlying Signaling Mechanisms

2.1 Introduction 3
- 2.1.1 Role of substrate stiffness in modulating cellular behavior 3
- 2.1.2 Cell differentiation vs reprogramming 3
- 2.1.3 Studying stiffness regulation of cellular reprogramming 4

2.2 Materials and Methods 5

2.3 Results 9
- 2.3.1 Intermediate substrate stiffness enhanced iN reprogramming efficiency 9
- 2.3.2 iNs produced on gels were mature and functional 12
- 2.3.3 Stiffness regulates SMAD signaling which correlates inversely with reprogramming efficiency 16
- 2.3.4 Biphasic dependence on stiffness can be generalized to single factor AsCl1-initiated neuron reprogramming 19
- 2.3.5 Parallel pathways act simultaneously at the early stage to enhance reprogramming 21

2.4 Discussion 25

Chapter 3: Extracellular Matrix from Human Amnion and Placenta as Biomaterials and their Effects on Cellular Fate

3.1 Introduction 27
- 3.1.1 Influence of extracellular matrix on cell fate 27
- 3.1.2 Tissue decellularization 27
- 3.1.3 Human amnion and placenta 28

3.2 Materials and Methods 29

3.3 Results 33
- 3.3.1 Optimized decellularization protocol removed cells but left ECM proteins intact 33
- 3.3.2 Non-collagenous and collagenous proteins could be sequentially extracted as separate fractions from tissues 33
- 3.3.3 *In vitro* characterization of placenta ECM on general cell properties 35

3.3.4 Effects of placenta ECM on maintenance of iPSCs 38
3.3.5 Placenta ECM forms a gel similar to Matrigel® at 37°C 40

3.4 Discussion 42

Chapter 4: Generation of a Novel Autologous Decellularized Extracellular Matrix Scaffold for Small Diameter Vascular Graft Replacement

4.1 Introduction 43
4.1.1 Vascular occlusion in small diameter vessels 43
4.1.2 Current clinical standards of care and challenges in small diameter graft replacement 43
4.1.3 Autologous biotubes as vascular grafts 43
4.1.4 Clinical trend – Acellular scaffolds as small diameter vascular grafts 44

4.2 Materials and Methods 45

4.3 Results 47
4.3.1 CHAPS is the optimal decellularization detergent for preparation of DAVGs 47
4.3.2 SDS is the optimal decellularization detergent for preparation of native aorta control 48

4.4 Discussion 51

Chapter 5: Concluding Remarks and Future Directions 52

References 53

List of Figures

Chapter 1

Figure 1.1 Bidirectional interaction between cells and biomaterials 1

Chapter 2

Figure 2.1 Intermediate substrate stiffness enhanced iN reprogramming efficiency 10

Figure 2.2 Adult mouse fibroblasts on 0.6 kPa gels were less metabolically active 11

Figure 2.3 BAM iNs on gels were mature similar to those on glass 13

Figure 2.4 Electrophysiology analysis indicating iN functionality 14

Figure 2.5 iNs generated were of the glutamatergic and GABAergic subtypes 15

Figure 2.6 Stiffness regulates SMAD signaling which correlates inversely with reprogramming efficiency 17

Figure 2.7 siRNA knockdown of SMURF2 18

Figure 2.8 Biphasic dependence of iN conversion efficiency on stiffness can be generalized to single factor AsCl1-initiated reprogramming 20

Figure 2.9 Stiffness regulates SMAD signaling which correlates inversely with reprogramming efficiency in AsCl1-initiated reprogramming, similar to BAM reprogramming 21

Figure 2.10 Parallel pathways act simultaneously at the early stage on intermediate stiffness to enhance reprogramming 22

Figure 2.11 RNA sequencing analysis for differential gene expression regulated by Ascl1 and stiffness 23

Figure 2.12 Summary of the effects of substrate stiffness on direct neuron reprogramming 24

Chapter 3

Figure 3.1 Collagenous and non-collagenous ECM proteins can be extracted sequentially as separate fractions from human placenta 34

Figure 3.2 Placenta ECM was compatible with cells and did not contain residual cytotoxic chemicals 36

Figure 3.3 Placenta ECM coating on culture surface did not affect cell phenotype 37

Figure 3.4 Placenta coating on culture surface can influence differentiation potential of cells 39

Figure 3.5 Placenta coating on culture surface is similar to Matrigel® and may have subtle effects on maintenance of pluripotent phenotype 40

Figure 3.6 Placenta ECM forms a gel similar to Matrigel® at 37°C 41

Chapter 4

Figure 4.1 Successful decellularization of DAVGs was obtained using CHAPS 48

Figure 4.2 Native aorta required sequential treatment with CHAPS and SDS for complete decellularization 49

Figure 4.3 SDS treatment was too harsh and caused structural damage to DAVGs 50

List of Tables

Chapter 2

Table 2.1 Antibodies used in immunocytochemistry 6

Table 2.2 Antibodies used in Western blotting 7

Table 2.3 Primers used in qRT-PCR 8

Table 2.4 Percentage of mature iNs relative to Tuj1 12

Chapter 3

Table 3.1 Antibodies used in Western blotting 30

Table 3.2 Antibodies used in immunocytochemistry 32

Table 3.3 Shear modulus and gelation time of Matrigel® and placenta ECM gel 41

Chapter 4

Table 4.1 Antibodies used in Western blotting 45

Chapter 1: Introduction

1.1 Dissertation Introduction

The microenvironment is known to influence cell fate and behavior. In turn, cells interact with and remodel their niches. *In vivo*, this microenvironment is mainly the extracellular matrix (ECM) that surrounds specific cell types in their niche and dynamic reciprocity between cells and ECM was first proposed by Bissell et al. in 1982[1]. *In vitro*, this is the material/s that cells interact with in adherent culture. The properties of biomaterials can be largely separated into two categories – biophysical properties and biochemical properties – each comprising additional subcomponents. This is detailed in Figure 1.1. These properties can provide instructional cues that result in changes in gene and protein expression in cells, thereby regulating cell state. As such, a comprehensive understanding of this bidirectional interaction is crucial to guide our design of next-generation biomaterials so as to be able to accurately control cell fate in a precise and predictable manner.

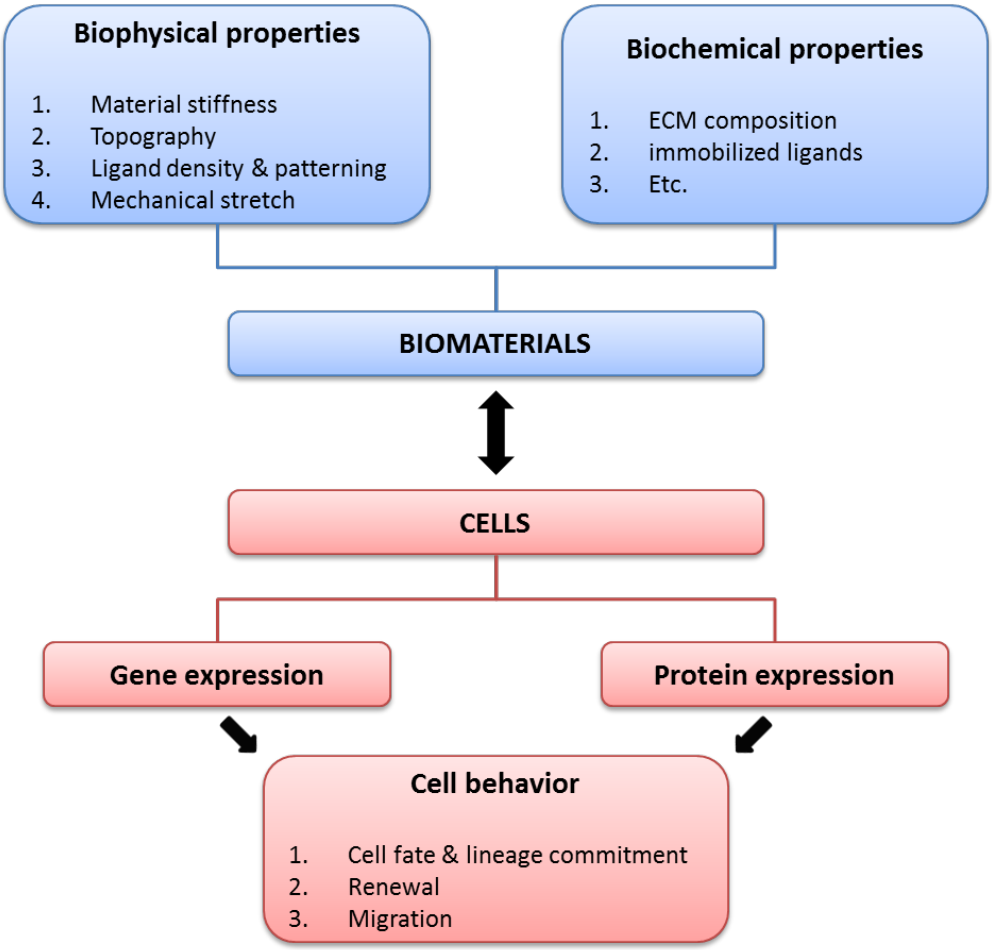

Figure 1.1 | Bidirectional interaction between cells and biomaterials. Biomaterial properties induce changes in cell behavior through changes in gene and protein expression.

1.2 Dissertation Outline

In this dissertation, we study the influence of biophysical and biochemical cues from biomaterials on adhesion cells. We attempt to better understand how these properties on adhesion substrates can be fine-tuned to more tightly control cell state.

In **Chapter 2**, we investigate the effects of biophysical properties in the cell microenvironment – in particular, material stiffness – on cell fate and lineage commitment during the process of direct reprogramming into neurons. We demonstrate, for the first time, that optimal substrate stiffness can modulate cell signaling pathways to positively influence the propensity of cells to become reprogrammed. In addition, we show that stiffness can replace small molecule inhibitors of these pathways commonly used to enhance the conversion efficiency. We also highlight the different effects of cell-material interaction in differentiation as opposed to reprogramming. These findings are critical to our understanding of the different roles material surface mechanics play in different cellular processes. It guides future design and optimization of biomaterials used in the creation of disease-specific models for drug screening.

In **Chapter 3**, we discuss the contribution of biochemical properties in the cell microenvironment – specifically, ECM composition – to cell fate in multipotent cardiac fibroblasts. Here, we isolate a complex ECM in soluble form from human term placentas and focus on the characterization of this material for biochemical composition and cyto-compatibility. We demonstrate that the type of ECM proteins can differentially influence the tendency of cell commitment towards different lineages. We also investigate the mechanical properties of this placenta ECM in a gel form for future potential *in vivo* use as an alternative to Matrigel®.

In **Chapter 4**, we generated a novel, autologous and acellular vascular graft composed of natural ECM proteins with potential clinical application as a small diameter vascular graft replacement, which traditionally has been the most challenging vascular graft application clinically. Here, we utilize the body's natural defense mechanism of forming fibrous capsules around foreign objects to generate a tissue tube around a cylindrical mandrel. This tissue is then decellularized and reimplanted as a vascular graft in an autologous manner. The emphasis of this chapter is on optimization of the decellularization protocol. We demonstrate that an optimized procedure can achieve maximum removal of cellular proteins and immunogenic nucleic acid components with minimal disruption to the ultrastructure of the ECM scaffold prior to re-implantation. This is crucial for *in vivo* graft remodeling and overall graft success.

Chapter 2: Biophysical Regulation of Direct Cell Reprogramming and the Underlying Signaling Mechanisms

2.1 Introduction

2.1.1 Role of substrate stiffness in modulating cellular behavior

Biophysical factors can include substrate stiffness, topography, ligand density and ligand density among many others. The work presented in this chapter focuses on the role of substrate stiffness in regulating cell behavior. Anchorage dependent cells can sense and respond to the rigidity of their underlying substrate[2]. Mathematically, substrate stiffness can be described by the modulus of elasticity E and is defined as tensile stress (force per unit area) divided by the corresponding strain (change in length over initial length). Much work has been done in the last 15 years studying the effect of substrate stiffness on cell morphology[3,4], adhesion[3], motility[5], proliferation[6], and even differentiation potentials[7–9] of various adult stem cells. These effects are known directly influence more complex biological processes like wound healing, tumor growth and cell lineage plasticity. We therefore hypothesize that it should also have implications in direct cell reprogramming. Yet, despite the extensive literature, there has yet to be any reports on the effect of substrate stiffness on the reprogramming process.

2.1.2 Cell differentiation vs reprogramming

Cell differentiation is the commitment of a relatively more potent cell towards a more defined lineage or cell type. Various degrees of cellular potency exists and cells can be totipotent, pluripotent, multipotent, oligopotent or unipotent. A totipotent cell can form any cell type of the body while a unipotent cell is terminally differentiated. Up till the first half of the 20th century, the prevalent view was that mature cells are permanently locked into a differentiated stage and it was impossible for them to return back to an immature, more pluripotent state. It wasn't until 1962 that John Gurdon first reported the reverse process is achievable by demonstrating that nuclei from terminally differentiated *Xenopus* intestinal epithelial cells were capable of generating full functional tadpoles upon transplantation into enucleated oocytes[10]. This reverse process is now known as reprogramming. In 2006, Takahashi and Yamanaka distilled the four core transcription factors *Oct4, Sox2, Klf-4* and *c-Myc*, capable of reprogramming any cell back to the pluripotent state and termed these the induced pluripotent stem cells[11]. This discovery opened up the possibility to generate much more easily any desired cell type from any starting cell by first reprogramming them back to the induced pluripotent stage and then differentiating them towards the target cell type. Direct reprogramming which as the name suggests is the direct conversion of cells into a completely different cell type without passing through the intermediate induced pluripotent stage has also been widely studied using specific transcription factors in a huge range of target cell types[12–17]. Direct reprogramming has wide applications in regenerative medicine, disease modeling and drug screening.

2.1.3 Studying stiffness regulation of cellular reprogramming

Although the roles of transcriptional factors[16–19], chemical compounds[20–22] and topographical cues[23] in direct reprogramming have been widely studied, the effects of extracellular matrix (ECM) and substrate stiffness on the reprogramming process are not well understood. By overexpressing transcriptional factors Brn2, Ascl1 and Myt1L[16], we used induced neuronal reprogramming as a model system to investigate how the mechanical property of the ECM modulates this process. We picked this system because it is robust and has been successfully repeated in numerous other labs.

2.2 Materials and Methods

Fibroblasts isolation, culture and reprogramming Ear tissues from adult C57BL/6 mice were isolated, minced and partially digested in Liberase™ (0.025mg/ml, Roche) for 45mins at 37°C. Partially digested tissues were plated and fibroblasts were allowed to migrate out (P0). Isolated fibroblasts were expanded in MEF medium (DMEM (Hyclone), 10%FBS (Hyclone) and 1% penicillin/streptomycin (GIBCO)) and used exclusively at P2 for all experiments. Fibroblasts were transduced and seeded onto polyacrylamide gels of varying stiffness. Medium was replaced 24hrs to MEF medium containing doxycycline (2ng/ml, Sigma) followed again by another medium change on day 2 to N3 medium (DMEM/F12 (Invitrogen), N2 supplement (Invitrogen), B27 supplement (Invitrogen), 1% penicillin/streptomycin and doxycycline (2ng/ml)). For Ascl1-only reprogramming, N3 medium was further supplemented with BDNF (5ng/ml, R&D systems) and GDNF (5ng/ml, R&D systems) after day 7. Cell metabolic activity was assayed using the PrestoBlue® Cell Viability Reagent (Invitrogen) with 12hr incubation at 24hrs post-seeding onto the various surfaces. Results were normalized to the number of cells adhered on each surface at 24hrs post-seeding. A8301 (0.5µM, Tocris) and K02288 (0.05µM, Tocris) were used for inhibition of SMAD phosphorylation. Unless otherwise stated, inhibitors were administered every other day for the first ten days in BAM reprogramming and for the first 14 days in Ascl1-only reprogramming. Reprogramming was done for a total of 14 days with BAM and 21 days with Ascl1 only. Half medium change was performed every 3 days in experiment sets without small molecule inhibitors or every 2 days in experiment sets with small molecule inhibitors.

Lentiviral production and transduction Doxycycline-inducible lentiviral vectors for Tet-O-FUW-Ascl1, Tet-O-FUW-Brn2, Tet-O-FUW-Myt1l and Tet-O-FUW-Ngn2 plasmids were used to transduce fibroblasts for ectopic expression of rtTA and Brn2, Ascl1, Myt1L (BAMR) or Ascl1 (AR) only. Lentivirus was produced using established calcium phosphate transfection methods. Viral particles were concentrated using Lenti-X Concentrator (Clontech) according to manufacturer's protocol. Stable virus was aliquoted and stored at -80°C. Fibroblasts were plated and allowed to attach overnight before viral transduction in the presence of polybrene (8µg/ml, Sigma). Cells were incubated with virus for 24hrs before seeding onto polyacrylamide gels.

Polyacrylamide gel fabrication Polyacrylamide gels were fabricated according to established protocols. Methacryloxypropyl-trimethoxysilane (Gelest), Sulfo-SANPAH (Thermo) and Laminin (5µg/cm^2, Corning) were used and gel thickness was 100µm. Gels of different stiffness were obtained by varying the ratio of acrylamide to bisacrylamide as previously documented[24].

Immunofluorescence and quantifications Samples were fixed in 4% paraformaldehyde, permeabilized in 0.25% Triton X-100 (Fisher) and blocked with 5% donkey serum (Sigma). Samples were incubated with primary antibodies (Refer to Table 2.1) overnight at 4°C followed by 1hr incubation with Alexa Fluor® 488- and/or Alexa Fluor® 546-conjugated secondary antibodies raised in donkey (Molecular Probes). Nuclei were stained with 4',6-diamino-2-phenylindole (DAPI; Invitrogen). Induced neurons were quantified under a Zeiss Axio Observer.D1. Criteria for a positive induced neuron was positive Tuj1 staining with circular cell body and an axon ≥3x length of cell body, as previously described[16] and reprogramming efficiency was determined as the % of induced neurons relative to the number of cells plated at 24hrs post-seeding. Epifluorescence images were collected using a Zeiss Axio Imager.A2.

Table 2.1 Antibodies used in immunocytochemistry

Antibody	Vendor	Catalog #	Dilution
Tuj1	Covance	MMS435P	1:1000
Tuj1	Covance	MRB435P	1:500
Tuj1	Abcam	AB18207	1:1000
MAP2	Sigma	M9942	1:200
NeuN	Covance	SIG39860	1:250
Synapsin	Abcam	Ab64581	1:200
VGlut1	Millipore	MAB5502	1:100
GABA	Sigma	A2052	1:500

Electrophysiology Samples were treated with a standard bath solution containing (in mM) 145 NaCl, 3 KCl, 10 HEPES, 3 $CaCl_2$, 8 glucose and 2 $MgCl_2$ at pH 7.4. Whole-cell recording was made using a patch clamp amplifier (MultiClamp 700B, Axon Instr.) under infrared differential interference contrast optics. Microelectrodes were made from borosilicate glass capillaries, with a resistance of 4-5 MΩ. For recording action potentials, cells were held at -70 mV in voltage-clamp mode. The intracellular solution for whole-cell recording of EPSPs and action potentials contained (in mM) 140 potassium gluconate, 5 KCl, 10 HEPES, 0.2 EGTA, 2 $MgCl_2$, 4 MgATP, 0.3 Na_2GTP and 10 Na_2-phosphocreatine at pH 7.2. For recording spontaneous excitatory postsynaptic currents (sEPSCs), cells were pre-treated with the extracellular bath solution containing 50 μM picrotoxin to exclude an inhibitory synaptic activity and held at -70mV in voltage-clamp mode with the intracellular solution containing (in mM) 130 $CsMeSO_4$, 7 CsCl, 10 HEPES, 1 EGTA, 4 MgATP, 0.3 Na_2GTP and 10 Na_2-phosphocreatine at pH 7.3. After recording basal sEPSC responses for 5 min, both 10 μM CNQX and 100 μM D,L-APV were applied to test a dependency of sEPSC responses on AMPA- and NMDA-type of glutamate receptors. For measuring spontaneous inhibitory postsynaptic currents (sIPSCs), cells were pre-treated with the bath solution containing 10 μM CNQX and 100 μM D,L-APV and held at -70mV with the intracellular solution containing (in mM) 137 CsCl, 10 HEPES, 1 EGTA, 4 MgATP, 0.3 Na_2GTP and 10 Na_2-phosphocreatine at pH 7.3. 50 μM picrotoxin was then added to test a dependency of sIPSC responses on GABA receptors after acquiring basal sIPSC responses for 5 min. Series resistance (15-30 MΩ) and input resistance (~200 MΩ using potassium-based internal solution; 1~2 GΩ using Cs-based internal solution) were monitored throughout the whole-cell recording or compared before and after sEPSC/IPSC recordings. Off-line analysis of spontaneous EPSC and IPSC were performed by using a threshold event detection function of Clampfit software (Molecular Devices).

Western blot Samples were cultured for 3 days before being lysed in buffer comprising 50mM Tris-HCl, 150mM NaCl, 0.5% Sodium deoxycholate, 1% SDS, 1% Triton X-100, 5% glycerol, 0.01% Bromophenol blue and protease inhibitors (phenylmethylsulfonyl fluoride, Na_3VO_4 and leupeptin). Lysates were boiled at 95°C for 5 mins and centrifuged to obtain the supernatant. Protein samples were relatively quantified by a trial run of equal volume loading, then probed for GAPDH to normalize for equal protein loading for future blots. Samples were separated on 10% SDS-PAGE gels, transferred to polyvinylidene difluoride membranes, blocked in 3% non-fat milk and incubated at 4°C overnight with primary antibodies (Refer to Table 2.2). Membranes were incubated with HRP-conjugated IgG secondary antibodies (Santa Cruz Biotechnologies, 1:2000) and protein bands visualized using Western Lightning Plus-Enhanced Chemiluminescence Substrate (Perkin Elmer Life & Analytical Sciences) on a digital imager (Bio-rad).

Table 2.2 Antibodies used in Western blotting

Antibody	Vendor	Catalog #	Dilution
pSMAD2/3	Cell Signaling	#8828	1:500
SMAD2/3	BD Biosciences	BD610843	1:500
pSMAD1/5/9	Cell Signaling	#9511, #13820	1:500
SMAD1	Cell Signaling	#6944	1:1000
SMURF2	Cell Signaling	#12024	1:1000
GAPDH	Abcam	Ab8245	1:2000
H3	Abcam	Ab1791	1:20000

RNA interference RNA interference was performed using non-targeting pool control (#D-001810-10 to -20) and ON-TARGETplus mouse SMURF2 (#J-064326-09 to -12) siRNAs from Dharmacon. Transfections were carried out using Lipofectamine® 2000 (Invitrogen) according to manufacturer's protocol.

RNA sequencing Samples were cultured for 3 days before being collected in Trizol® (Ambion) and RNA extracted according to manufacturer's protocol. A total of 500ng total RNA was subjected to poly A selection using the Dynabeads® mRNA DIRECT™ kit (Invitrogen) followed by library preparation using the PrepX RNA-Seq for Illumina Library Kit (Wafergen) before sequencing on the HiSeq4000 (Illumina) at 50 single-read runs. Mouse annotations were obtained for R and the Gage and Pathview Bioconductor Packages were used respectively to determine overexpressed pathways and to map pathways. Differential expression was analyzed using DESeq2.

qRT-PCR Samples for qRT-PCR were cultured for 3 days before being collected in Trizol® (Ambion) and RNA extracted according to manufacturer's protocol. A total of 500ng total RNA was reverse transcribed into cDNA using Maxima First Strand cDNA Synthesis Kit (Thermo). Template DNA was amplified using Maxima SYBR Green/Fluorescein qPCR Master Mix (Thermo) on a CFX qPCR machine (Bio-rad). Gene expression levels were normalized to 18S and mouse brain were used as calibration control. Primers used are detailed in Table 2.3.

Table 2.3 Primers used in qRT-PCR

Gene	Forward primer	Reverse primer
SMAD1	TCAGCCCATGGACACGAA	CCTGAACATCTCCTCTGCTGATT
SMAD2	AGCCTCCCGGAGGGTAGA	GATGGACGACATTTTCTTACCAAA
SMAD3	CAGAAGGCCGGCT CACAGTA	CAGCACACAATAACTTGGACCTACA
TGFβ1	GCCTGAGTGGCTGTCTTTTGA	TGTATTCCGTCTCCTTGGTTCA
TGFβR1	CGCGCTGACATCTATGCAAT	TCATGGATTCCACCAATAGAACAG
SMURF2	TGGGGACATGTCTAACCCC	TTTTGCACAGAGTACTGTCAGG
Brn2	AGGGCGCAAACGGAAAA	GGCTTAGGGCATTTGAGGAAA
Myt1L	CTACAAGATGGACGTGGACTCTGA	GGAACTCGAACCCCTTTGG

Statistical analysis All data are presented as mean ± one standard deviation. Comparisons among values for groups greater than two were performed using a one-way analysis of variance (ANOVA) followed by Dunnett's post-hoc test. For all cases, p-values less than 0.05 were considered statistically significant. GraphPad Prism® 6.0 software was used for all statistical evaluations.

2.3 Results

2.3.1 Intermediate substrate stiffness enhanced iN reprogramming efficiency

We hypothesize that stiffness has implications on direct cell reprogramming. To test our hypothesis, adult mouse ear fibroblasts transduced with doxycycline-inducible lentiviral vectors for BAM were seeded onto polyacrylamide gels of various stiffness (0.6 kPa, 8 kPa, 20 kPa and 40 kPa), including glass coverslips conjugated with the same ECM proteins as a reference. Cells were maintained in N3 medium for 14 days before immunostaining and quantifying for reprogramming efficiency (Fig. 2.1a). iNs were observed on all surfaces (Fig. 2.1b and Fig. 2.3). Interestingly, we observed a biphasic trend with the intermediate stiffness of 20 kPa being the most efficient for direct reprogramming into neurons, independent of the ECM proteins conjugated on the gels (Fig. 2.1c). Considering that laminin is known to: 1) play a crucial role during development of the nervous system[25], 2) promote neurite regeneration[26] and 3) facilitate neurite growth better than collagen or fibronectin[27], laminin was used in all further studies. In addition, because we observed that fibroblast morphology was distinctly different and metabolic activity was significantly lower on the 0.6 kPa gels compared to all other surfaces (Fig. 2.2a), 0.6 kPa was replaced by 1 kPa gels in all experiments going forward. This change did not affect the biphasic trend (Fig. 2.2b).

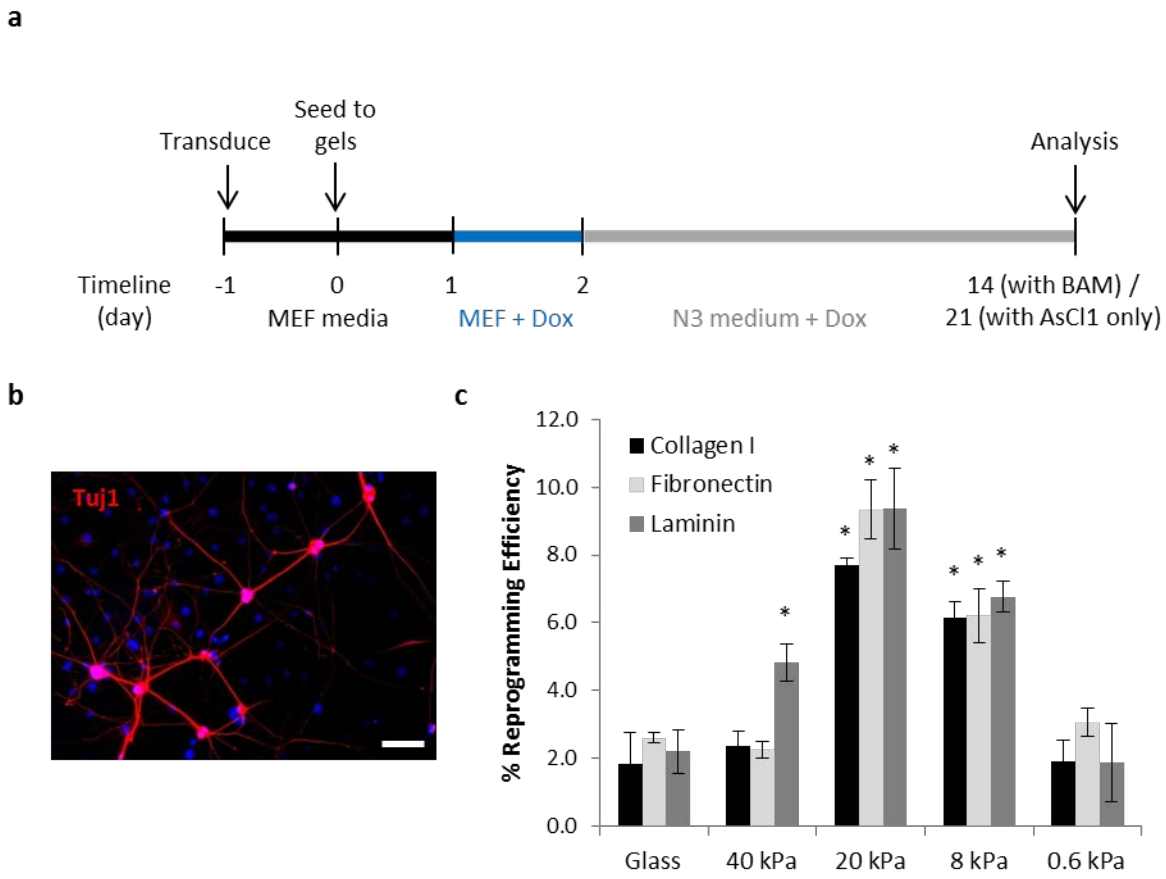

Figure 2.1 | Intermediate substrate stiffness enhanced iN reprogramming efficiency. a, Reprogramming timeline. Cultures were maintained in N3 medium with doxycycline for 14 or 21 days respectively when reprogramming with BAM or Ascl1 alone. **b**, Representative image of iNs from BAM reprogramming on 20 kPa gels. iNs were positive for Tuj1 and formed networks (scale bar, 100µm). **c**, Reprogramming efficiency of adult fibroblasts transduced with BAM cultured on polyacrylamide gels of various stiffness and glass as reference. Bar graphs represent mean ± one standard deviation, n = 3. Statistical significance determined by one-way ANOVA followed by Dunnett's post-hoc test, *$p \leq 0.05$ compared to glass with the same ECM protein.

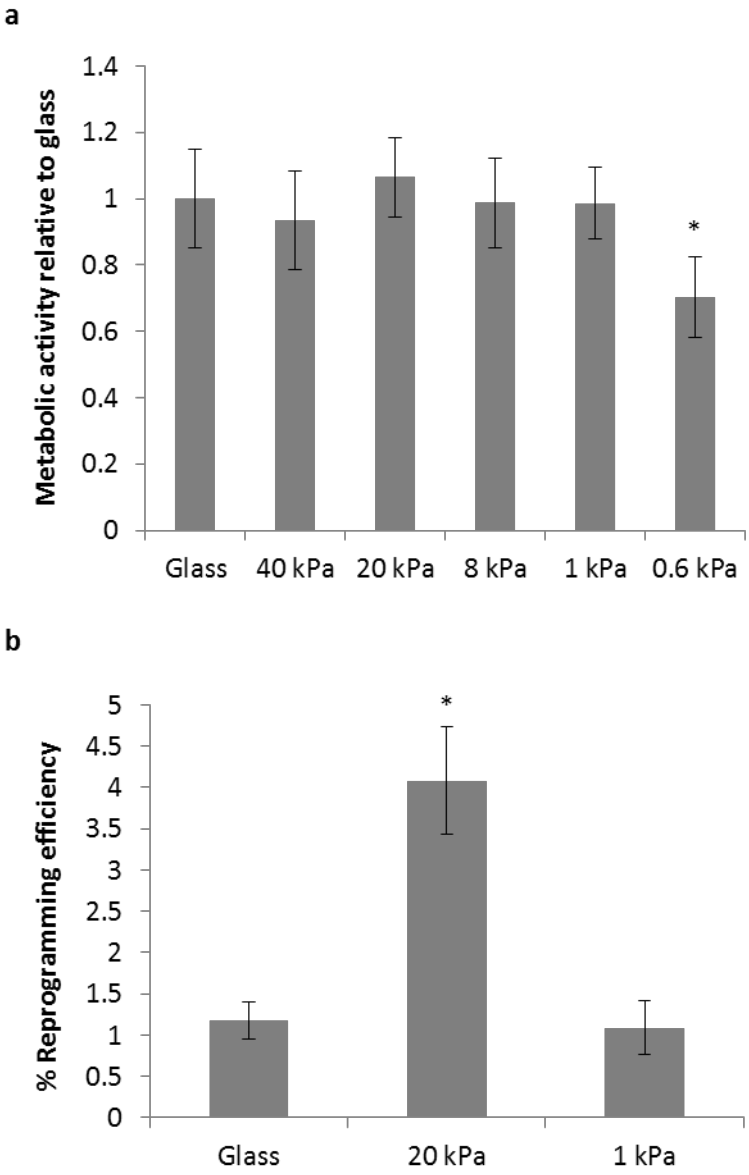

Figure 2.2 | Adult mouse fibroblasts on 0.6 kPa gels were less metabolically active. a, Relative metabolic activity of cells cultured on polyacrylamide gels of various stiffness relative to glass as determined by the PrestoBlue® Cell Viability Reagent. Bar graphs represent mean ± one standard deviation, n = 3. Statistical significance determined by one-way ANOVA followed by Dunnett's post-hoc test, $*p \leq 0.05$ compared to glass. **b**, Replacement of 0.6 kPa gels with 1 kPa gels resulted in no change in biphasic trend. Reprogramming efficiency of BAM-transduced adult mouse fibroblasts cultured on glass, 20 kPa and 1 kPa gels. Bar graphs represent mean ± one standard deviation, n = 6. Statistical significance determined by one-way ANOVA followed by Dunnett's post-hoc test, $*p \leq 0.05$ compared to glass.

2.3.2 iNs produced on gels were mature and functional

iNs on gels were mature (Table 2.4) and exhibited positive staining for MAP2, NeuN and synapsin (Fig. 2.3). Electrophysiology analysis showed the induced neurons to be functional, exhibiting spontaneous changes in membrane potential in response to current injection (Fig. 2.4a). Although similar number of action potentials were generated across all groups (Fig. 2.4b), we found significantly higher frequency of spontaneous excitatory post synaptic currents (sEPSC) generated on the 20 kPa samples compared to all other stiffness (Fig. 2.4c) presumably due to the higher number of iNs formed on the intermediate stiffness. No significant difference in spontaneous inhibitory post synaptic currents (sIPSC) frequency was observed (Fig. 2.4d). Representative sEPSC and sIPSC traces across all stiffness are shown in Fig. 4e.

Table 2.4 Percentage of mature iNs relative to Tuj1

% Double positive	Glass	20 kPa	1 kPa
MAP2/Tuj1	98.4 ± 1.0	98.3 ± 1.3	98.6 ± 1.3
NeuN/Tuj1	98.4 ± 0.7	99.2 ± 0.3	98.2 ± 1.0
Synapsin/Tuj1	97.8 ± 1.0	98.8 ± 1.1	97.7 ± 1.5

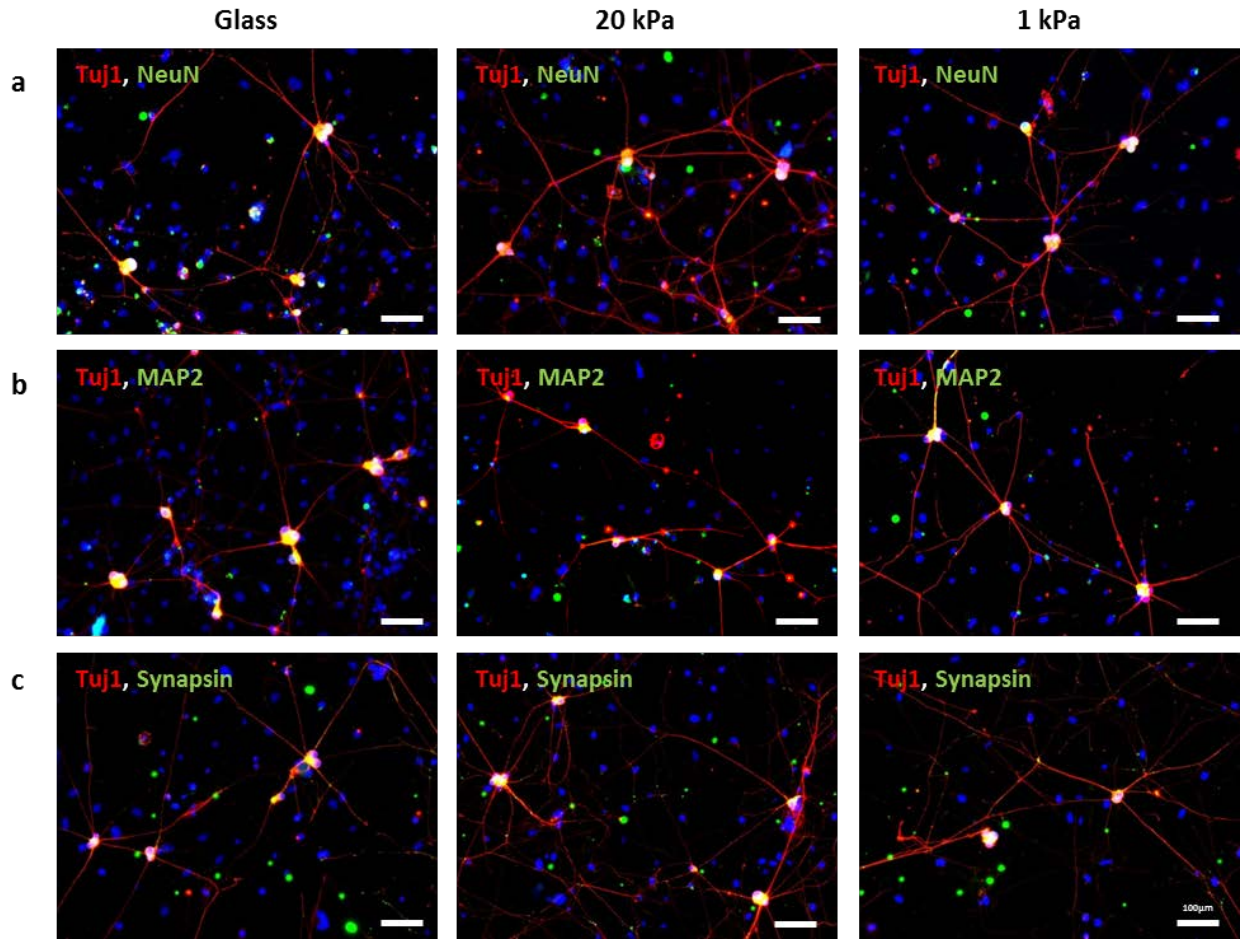

Figure 2.3 | BAM iNs on gels were mature similar to those on glass. Representative immunostaining images of iNs on glass and 1 kPa gels for mature neuronal markers **a**, NeuN **b**, MAP2 and **c**, Synapsin (scale bar, 100µm).

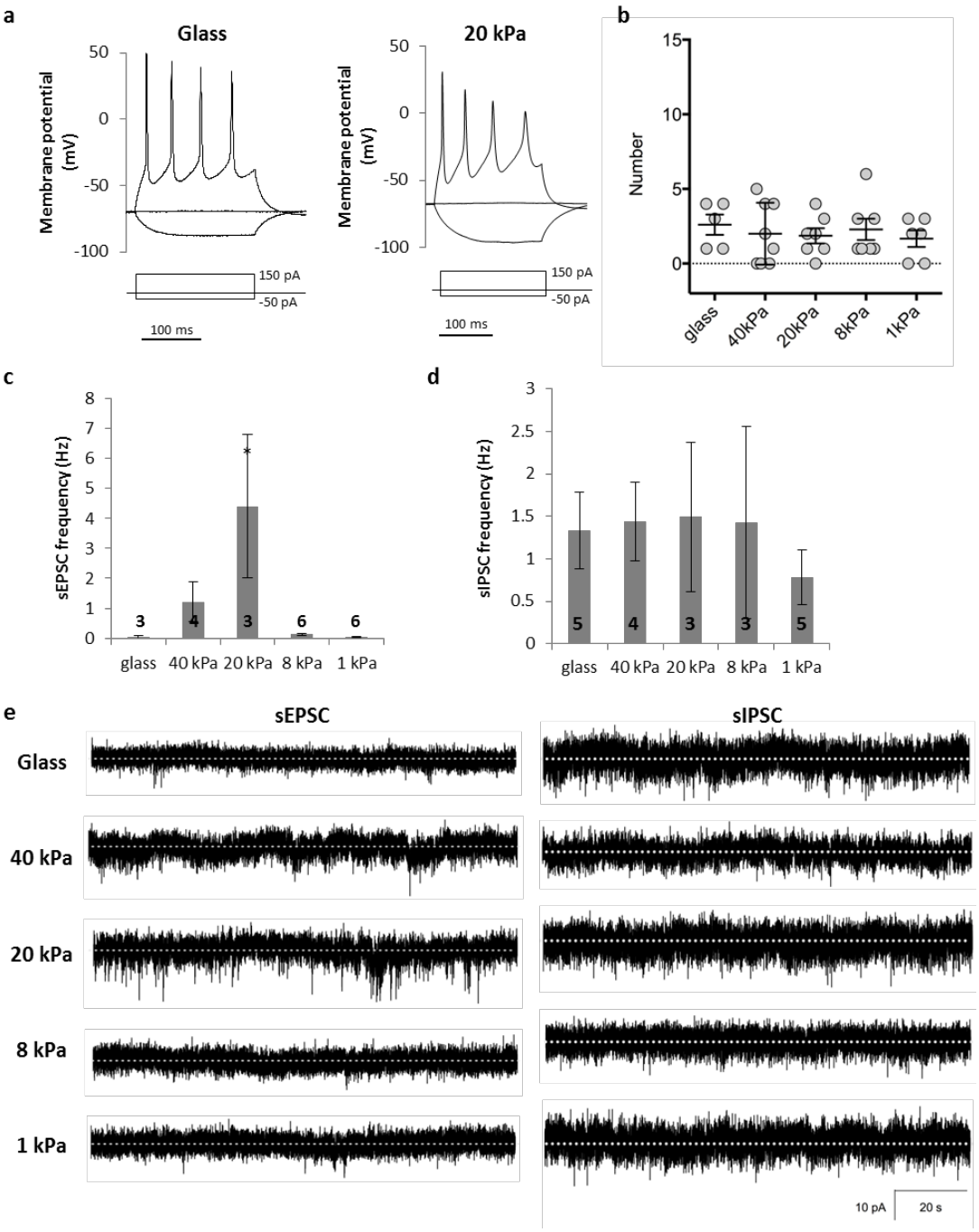

Figure 2.4 | Electrophysiology analysis indicating iN functionality. a, Representative trace showing spontaneous changes in membrane potential in response to current injection from iNs on glass and 20 kPa gels. **b**, Number of action potentials generated per iN across all stiffness. Each circle represents one cell tested. **c**, Quantification of sEPSC frequency of iNs across all stiffness. **d**, Quantification of sIPSC frequency of iNs across all stiffness. For **b**, **c** and **d**, bar graphs represent mean ± one standard error of mean, number of iNs tested as stated. Statistical significance determined by one-way ANOVA followed by Dunnett's post-hoc test, $*p \leq 0.05$ compared to glass. **e**, Representative sEPSC and sIPSC traces generated from iNs across all surfaces.

Further characterization found the iNs to be of the GABAergic and glutamatergic subtypes (Fig. 2.5), in agreement with reported literature for iN reprogrammed with BAM[16]. We did not observe any significant difference in neuronal subtype expression between different substrate stiffness. In short, intermediate substrate stiffness of ~20 kPa enhanced direct neuron reprogramming efficiency compared to stiffer and softer substrates and produced iNs that were both mature and functional.

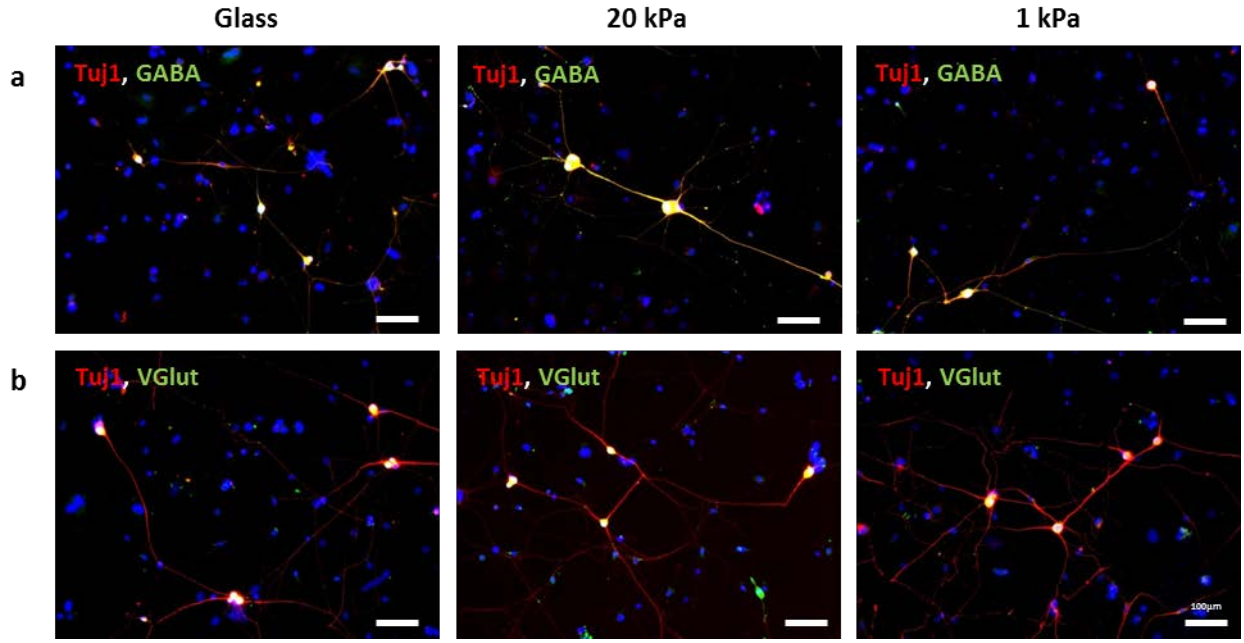

Figure 2.5 | iNs generated were of the glutamatergic and GABAergic subtypes. Immunostaining images of iNs on glass, 20 kPa and 1 kPa gels for mature neuronal subtypes **a**, GABA and **b**, VGlut (scale bar, 100µm).

2.3.3 Stiffness regulates SMAD signaling which correlates inversely with reprogramming efficiency

We postulate that the effects of substrate stiffness on iN reprogramming efficiency were due to alterations in downstream, mechanosensitive pathways. To test this, we analyzed expression of key proteins in pathways which have been linked to a mechanical response or lineage commitment. Of those tested, we observed with great interest a biphasic trend in both total protein expression and phosphorylation of SMAD2/3 (Fig. 2.6a). On the other hand, SMAD1 total protein expression remained similar across stiffness and only phosphorylation varied. We did not observe a biphasic gene expression level (Fig. 2.6b).

Classical SMAD signaling primarily involves two arms with TGFβ ligands signaling though receptor-regulated SMADs (R-SMAD) 2/3 and BMP ligands signaling through R-SMAD1/5/9. Activation causes the ALK receptors to phosphorylate R-SMADs leading to their translocation into the nucleus to activate gene transcription. To determine whether substrate stiffness and SMAD signaling had similar effects on direct neuron reprogramming, we performed reprogramming on different substrate stiffness in the presence and absence of A8301 and K02288. These are small molecule inhibitors of the ALK receptors, with the former inhibiting TGFβ and the latter BMP signaling, that function by inhibiting phosphorylation of the respective R-SMADs. Interestingly, addition of A8301 and K02288 together significantly enhanced the reprogramming efficiency on the stiffest and softest substrates to a similar level as that on the intermediate stiffness without inhibitors (Fig. 2.6c). Moreover, the addition of both inhibitors to cultures on the intermediate stiffness did not further increase reprogramming efficiency, suggesting that they might share a similar pathway in improving the efficiency.

Given that we did not observe a biphasic gene expression level (Fig. 2.6b), we hypothesized that the low expression of SMAD2/3 at intermediate stiffness was a result of enhanced degradation. To further confirm the role of SMAD degradation in substrate stiffness-enhanced neuron reprogramming, we used siRNA against SMAD-specific ubiquitination regulatory factors (SMURFs). SMURF 2 decreases expression of SMADs 1 and 2 to suppress both BMP and TGFβ signaling[28]. Knockdown of SMURF 2 was confirmed at both the protein and gene expression levels (Fig. 2.7). Knockdown is expected to prevent degradation and lead to the accumulation of SMADs 1 and 2. Indeed, addition of si-SMURF 2 attenuated the reprogramming efficiency on the intermediate stiffness to the basal level (Fig. 2.6d). Altogether, our results demonstrate that substrate stiffness mediates SMAD signaling to influence direct neuron reprogramming.

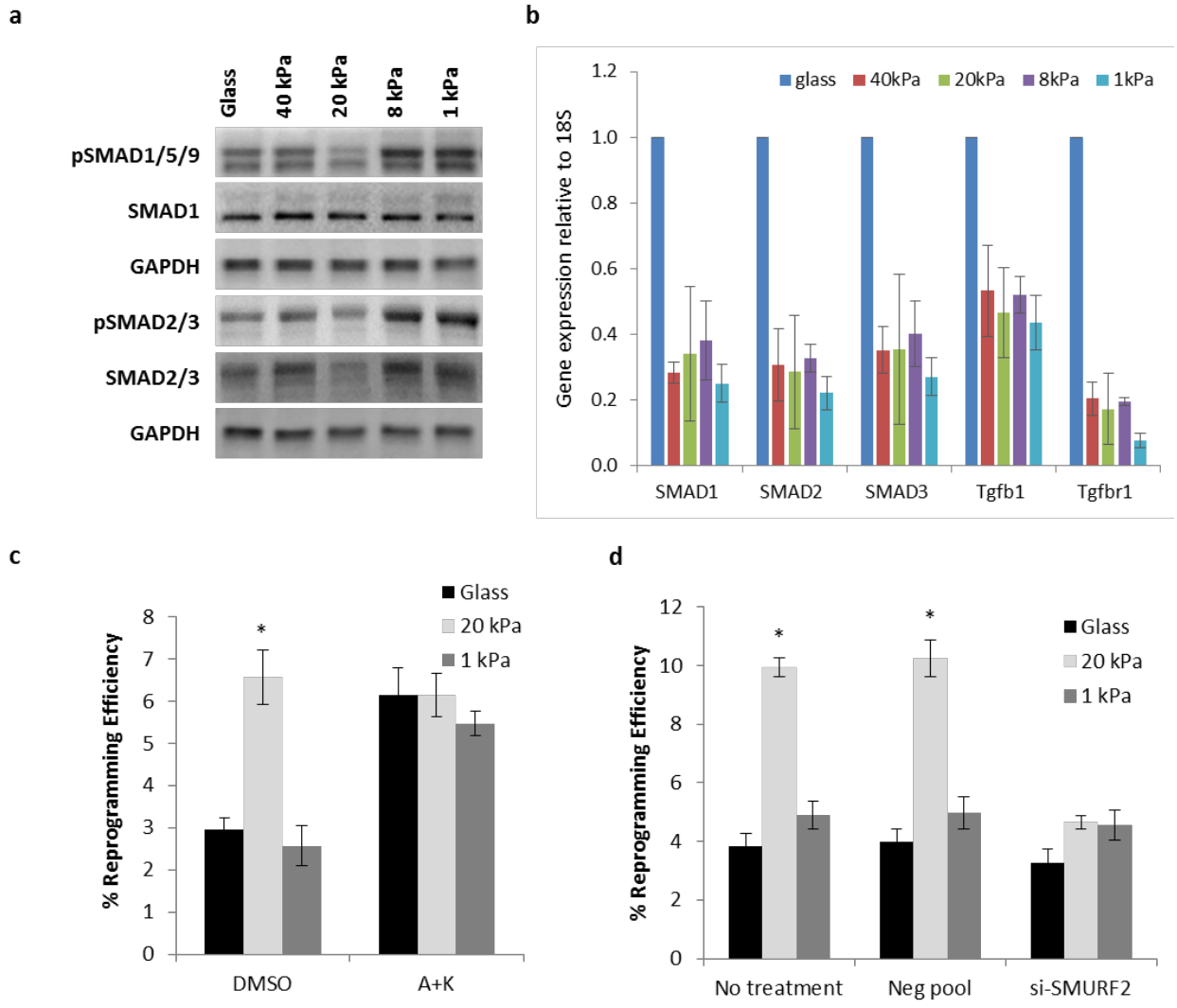

Figure 2.6 | Stiffness regulates SMAD signaling which correlates inversely with reprogramming efficiency. **a**, Western blot analysis for SMAD proteins in adult mouse fibroblasts cultured on glass or polyacrylamide gels of various stiffness. GAPDH shown as loading control. **b**, Gene expression analysis of key components of the SMAD pathway - SMAD1, SMAD2, SMAD3, TGFβ1 and TGFβR1 on gels relative to glass reference, normalized to 18S. **c**, Reprogramming efficiency of BAM-transduced adult fibroblasts in the presence of A8301 and K02288. **d**, Reprogramming efficiency of BAM-transduced adult fibroblasts after knockdown of SMAD-specific ubiquitination regulatory factor 2 (SMURF 2). For **b, c** and **d**, bar graphs represent mean ± one standard deviation, n = 3. Statistical significance determined by one-way ANOVA followed by Dunnett's post-hoc test, $*p \leq 0.05$ compared to glass reference within the same treatment group.

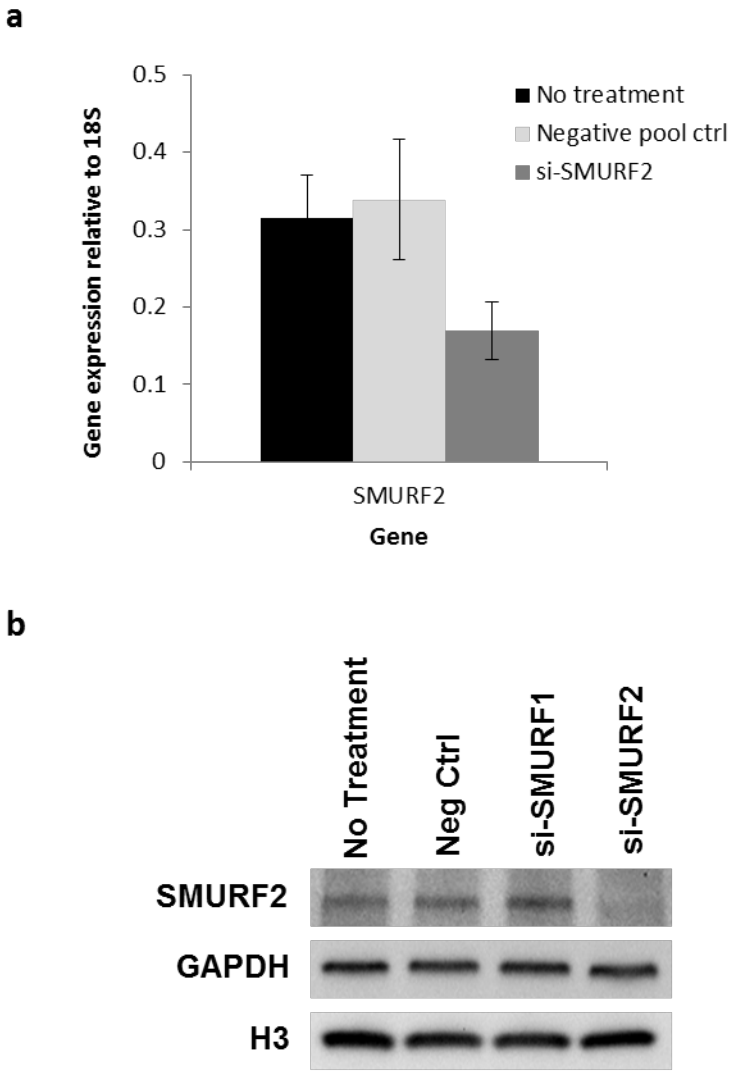

Figure 2.7 | siRNA knockdown of SMURF2. a, qRT-PCR expression analysis of SMURF2 RNA interference with gene expression normalized to 18S. Bar graphs represent mean ± one standard deviation, n = 3. Statistical significance determined by one-way ANOVA followed by Dunnett's post-hoc test, $*p \leq 0.05$ compared to non-treated control within the same treatment group. **b**, Western blot confirming successful knockdown.

2.3.4 Biphasic dependence on stiffness can be generalized to single factor AsCl1-initiated neuron reprogramming

The key role of Ascl1 in the neuron reprogramming cocktail had previously been demonstrated by the lack of iNs when reprogramming with only Brn2 and Myt1L. Moreover, Ascl1 alone was proven to be able to generate iNs when co-cultured with glial cells while Brn2 and Myt1L functioned primarily in iN maturation[29]. We were thus curious to see if the biphasic effect of substrate stiffness still holds when reprogramming with Ascl1 only. Remarkably, we observed an even more dramatic effect in single factor reprogramming (Fig. 2.8a). iNs generated with Ascl1 were mature, with glutamatergic and GABAergic neurons as the main neuronal subtypes (Fig. 2.8b-d). Protein expressions across substrate stiffness were tested next and the biphasic expression and phosphorylation of SMAD2/3 and SMAD1/5/9 were consistent with that in BAM reprogramming (Fig. 2.9a). As shown before, SMAD phosphorylation correlates inversely with reprogramming efficiency (Fig. 2.9b). Taken together, our results confirm that whether with Ascl1 alone or with all three reprogramming factors BAM, low SMAD phosphorylation on intermediate stiffness suppresses SMAD signaling to result in higher direct neuron reprogramming efficiency.

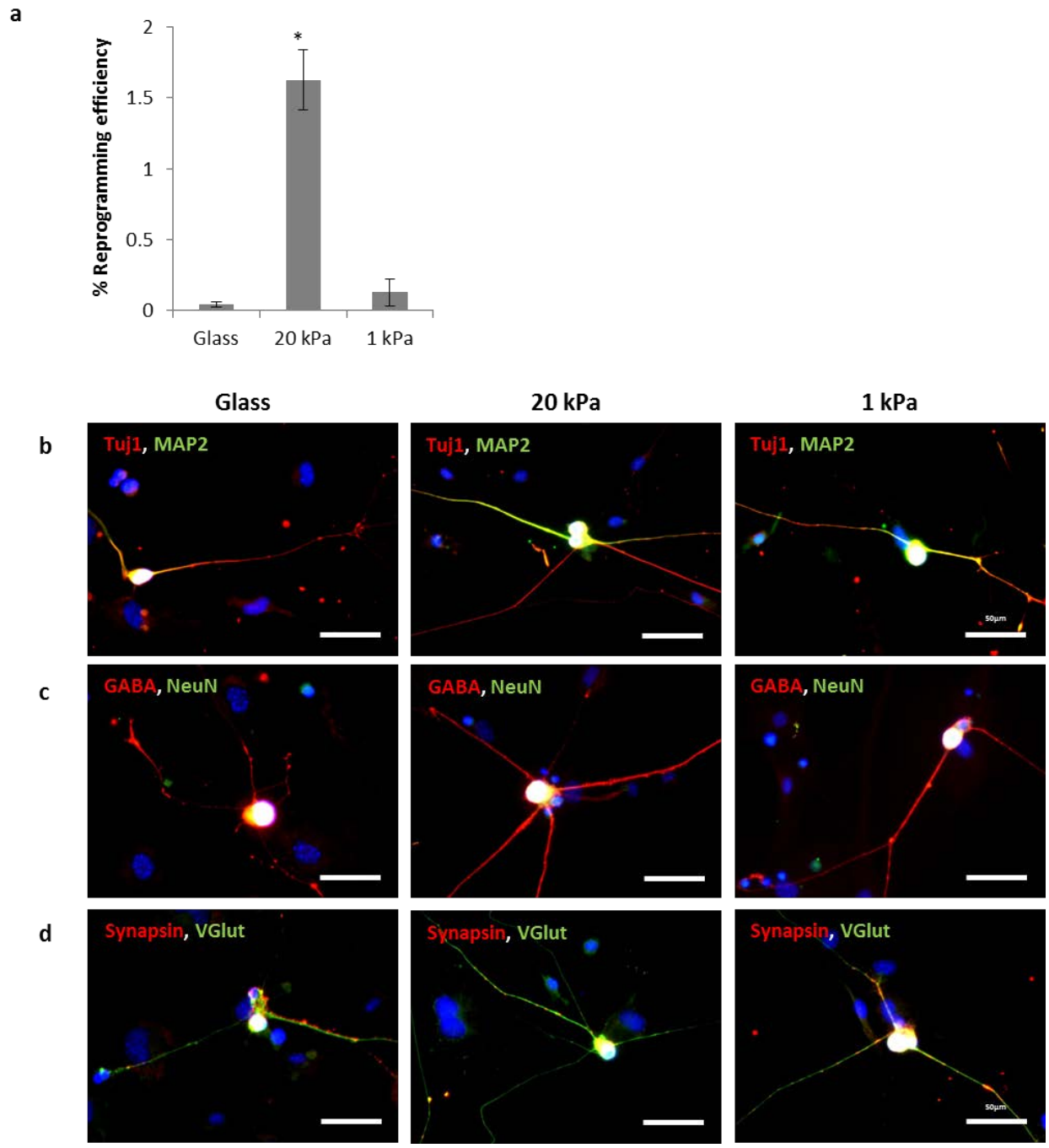

Figure 2.8 | Biphasic dependence of iN conversion efficiency on stiffness can be generalized to single factor AsCl1-initiated reprogramming. a, Reprogramming efficiency of adult fibroblasts transduced with Ascl1 alone cultured on polyacrylamide gels and glass. Bar graphs represent mean ± one standard deviation, n = 3. Statistical significance determined by one-way ANOVA followed by Dunnett's post-hoc test, $*p \leq 0.05$ compared to glass. **b**, Representative immunostaining images of iNs from single factor Ascl1 reprogramming on glass, 20 kPa and 1 kPa gels showing neuronal maturity and subtypes similar to BAM reprogramming (scale bar, 50µm).

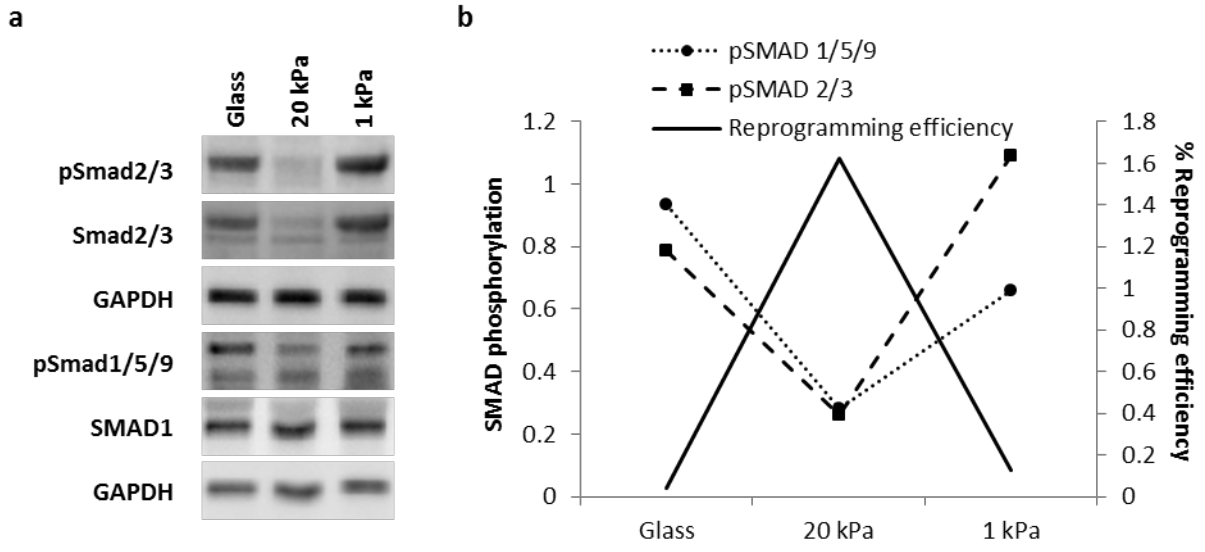

Figure 2.9 | Stiffness regulates SMAD signaling which correlates inversely with reprogramming efficiency in AsCl1-initiated reprogramming, similar to BAM reprogramming. **a**, Western blotting analysis of Ascl1-transduced adult mouse fibroblasts cultured on glass or gels. **b**, Combined plots of phospho-SMAD quantity with single factor reprogramming efficiency, demonstrating inverse correlation.

2.3.5 Parallel pathways act simultaneously at the early stage to enhance reprogramming

We then sought to understand the more dramatic biphasic trend in Ascl1-only-mediated reprogramming efficiency. Considering that we had observed reprogramming efficiency on the glass controls in the three factor system to be much higher than the controls in the single factor system, we questioned if perhaps the intermediate stiffness facilitated an upregulation of Brn2 and Myt1L by Ascl1. We utilized qRT-PCR to probe changes in gene expression in Ascl1-transduced cells and indeed observed the upregulation of endogenous Brn2 and Myt1L on intermediate stiffness (Fig. 2.10a). This upregulation was not seen in non-transduced cells (data not shown).

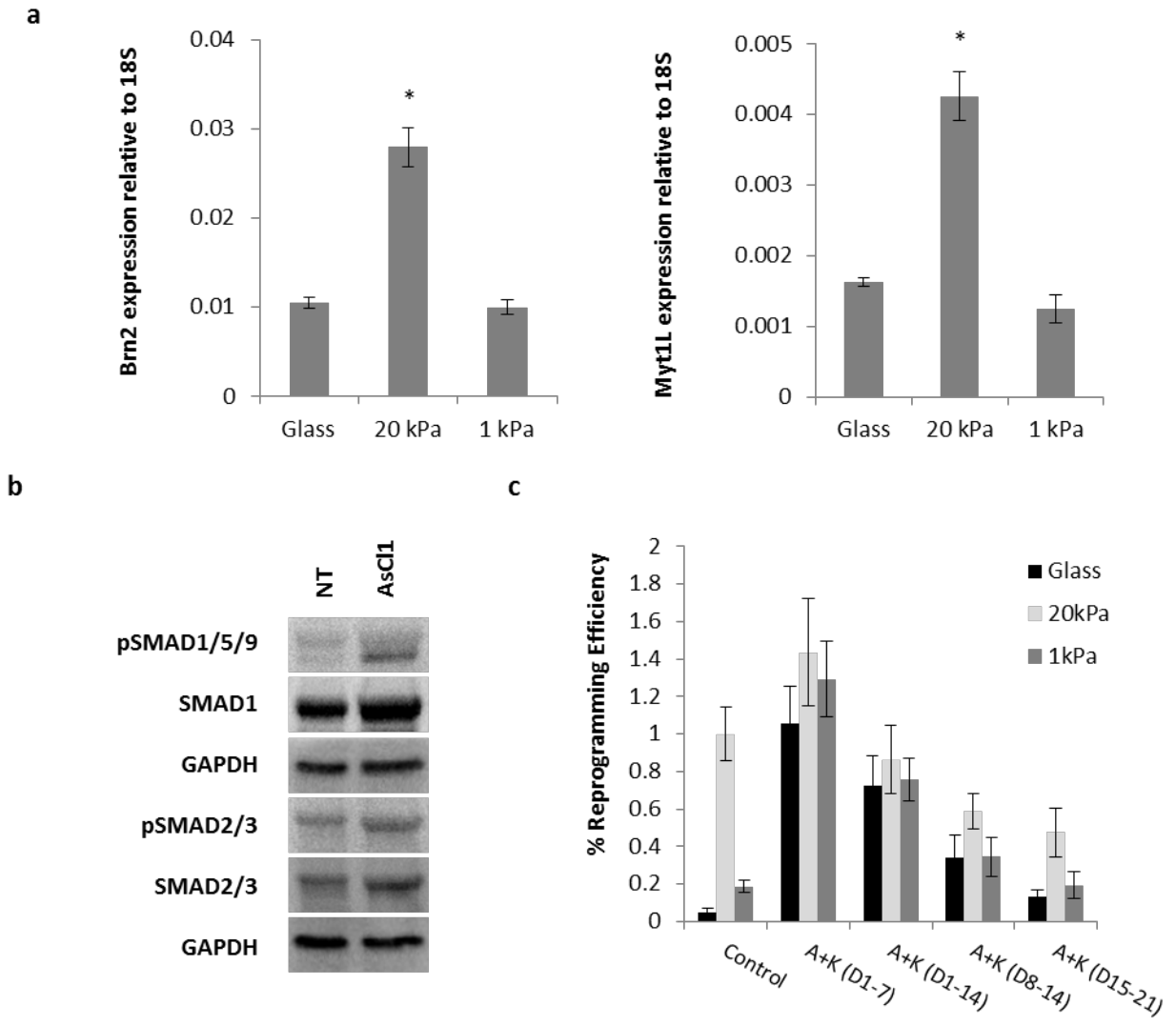

Figure 2.10 | Parallel pathways act simultaneously at the early stage on intermediate stiffness to enhance reprogramming. **a**, qRT-PCR analysis of Ascl1-transduced adult mouse fibroblasts for Brn2 and Myt1L expression. Bar graphs represent mean ± one standard deviation, n = 3. Statistical significance determined by one-way ANOVA followed by Dunnett's post-hoc test, $*p \leq 0.05$ compared to glass. **b**, Western blot analysis comparing SMAD expression in non-transfected (NT) and AsCl1-transfected cells cultured on tissue culture dish. **c**, Temporal kinetic analysis of SMAD inhibition on Ascl1 reprogramming. Bar graphs represent mean ± one standard deviation, n = 3.

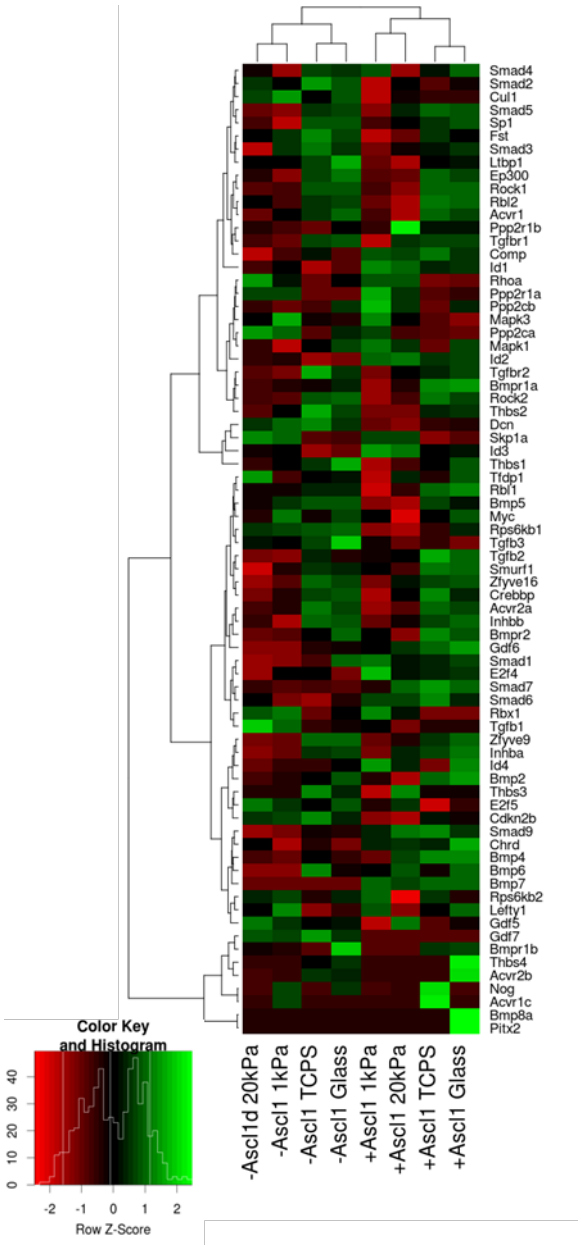

Figure 2.11 | RNA sequencing analysis for differential gene expression regulated by Ascl1 and stiffness. Gene heatmap for regularized log transform for expression of selected genes related to the TGFβ pathway. Coloring represents sample row-wise z-score. (Credits to Douglas O Kelkhoff)

We then further determined the effects of Ascl1 transfection on downstream gene expression and thereafter performed RNA sequencing to compare gene expression in non-transfected and Ascl1-transfected cells to gain insights into any pathways that may be involved. RNAseq analysis for differential expression revealed the major pathways regulated by the forced expression of Ascl1 and stiffness. Of particular interest, genes related to the TGFβ pathway were observed to be

highly differentially expressed. Based on the clustering analysis, Ascl1 had dominant effects on the TGFβ pathway using genes associated with the respective PIR functional categories within DAVID[30,31] (Fig. 2.11). Upon comparing protein expression in non-transfected and Ascl1-transfected cells, we found that Ascl1 activated SMAD signaling, as indicated by the higher levels of expression for both phosphorylated and total SMAD proteins in transfected cells (Fig. 2.10b).

Addition of A8301 and K02288 inhibitors was again able to rescue reprogramming on both the stiff and soft surface to become comparable to that on the intermediate stiffness, thus confirming the role of substrate stiffness in regulating SMAD signaling (Fig. 2.10e). In addition, because reprogramming is suggested to involve the sequential fulfilment of two phases[21,32] – the downregulation of the source cell phenotype and induction of the target cell phenotype – we further investigated whether the temporal regulation of SMAD signaling was critical to its impact in driving neuronal reprogramming. We thus set out to understand the temporal effects of SMAD inhibition by adding A8301 and K02288 during the early (D1-7), mid (D8-14) and late (D15-21) phase of Ascl1-only reprogramming. Interestingly, inhibition of SMAD signaling appears to be most crucial only in the early phase of reprogramming. In contrast, mid and late phase SMAD inhibition seemed to have no significant effect (Fig. 2.10e). In summary, our findings highlight that SMAD inhibition is time-sensitive and most effective in the early phase of reprogramming. The effects of substrate stiffness on induced neuronal reprogramming are summarized in Figure 2.12.

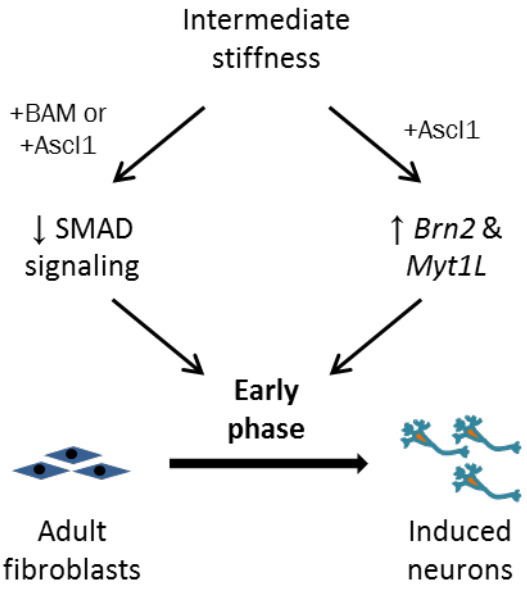

Figure 2.12 | Summary of the effects of substrate stiffness on direct neuron reprogramming.

2.4 Discussion

Our work highlights, for the first time, a biphasic dependence of direct reprogramming on substrate stiffness. It is especially interesting that the intermediate stiffness is optimal for direct reprogramming, considering it is well established that soft substrates are most conducive for neuronal differentiation[7,8]. This clearly demonstrates that differentiation and reprogramming are two very different processes besides the difference in the starting cell type. Previous study by Sun et al. showed that soft substrates (<5 kPa) containing micropost array suppressed TGFβ signaling in neural stem cells to facilitate the differentiation into motor neurons[25]. In contrast, we observed an activation of TGFβ signaling in fibroblasts on soft flat substrates (1 kPa). Apart from the different cell types, it is possible that signaling pathways activated/inhibited in cells on smooth/flat surfaces differ from those on microtopographic substrates.

Our data suggest SMAD signaling is a key stiffness-regulated pathway and SMAD inhibition in the early phases of reprogramming can enhance the conversion efficiency. Consistently, activation of the BMP pathway had previously been reported to inhibit neuron differentiation[33] and neurogenesis by causing the degradation of transcription factor Ascl1[34], which was recently suggested to be a pioneer factor essential for initiating the direct reprogramming process from fibroblasts to neurons[35]. In addition, inhibition of BMP signaling in Ngn2-driven neuron reprogramming[36] and TGFβ signaling in small molecule-driven reprogramming[21] were also found to aid neuronal survival and maturation. These results suggest that intermediate substrate stiffness could be used to replace these biochemical factors to enhance the conversion of fibroblasts into iNs. The activation of SMAD signaling by Ascl1 alone is unexpected, and the more dramatic enhancement of conversion efficiency by intermediate stiffness further highlights the beneficial effect of suppressing SMAD signaling by the mechanical property of the substrate.

While early SMAD inhibition enhanced iN conversion in our system, this enhancement was not seen in mid-late phase inhibition. However, Hu and colleagues had observed the contrary where SMAD inhibition was not essential in the early phase of chemical reprogramming but was added later to facilitate neuronal survival and maturation[22]. We think this can be attributed to a few possible reasons: 1) the key drivers of reprogramming are different between Ascl1-directed neuron reprogramming system and small molecule-driven reprogramming, 2) on the basis that we had observed immature neurons in our cultures by day 5 post-doxycycline induction, it is possible that SMAD inhibition facilitates the early phase of direct neuron reprogramming before switching to play a critical role in mid-late phase survival and maturation of iNs, 3) cell type and species are different and 4) this decline may simply be a result of drug toxicity to iNs. Regardless, this suggests that the reprogramming process is a series of finely orchestrated events occurring at different time points.

In summary, these findings are critical to our understanding of cell lineage plasticity in response to surface mechanics for the optimization of biomaterials for cell-engineering applications, with potential applications in the creation of disease-specific models for drug screening. Our results demonstrate that optimizing substrate stiffness can significantly enhance direct reprogramming efficiency. The biphasic effect of substrate stiffness on neuron reprogramming efficiency is surprising considering it is well established by now that soft substrates comparable to the native stiffness of the brain typically facilitates upregulation of neuronal genes and are more favorable

for neuronal differentiation. Moreover, this highlights the different underlying mechanisms for stem cell differentiation and cell reprogramming, which await further investigations.

Chapter 3: Extracellular Matrix from Human Amnion and Placenta as Biomaterials and their Effects on Cell Fate

3.1 Introduction

3.1.1 Influence of extracellular matrix on cell fate

The microenvironment of cells is long known to have effects on cellular behavior. The microenvironment, apart from the biophysical factors mentioned in the previous chapter, also includes the ECM proteins present, their specific biochemical composition, density and organization. This is not surprising considering that the ECM is not the same in all organs around the body. Apart from simply facilitating cell adhesion, a vast amount of literature exists to suggest that the specific ECM present in the microenvironment of cells can also influence cell fate. Since the 1980s, ECM has been demonstrated in mouse mammary epithelial cells to play a critical role in the maintenance of tissue-specific function in culture[37]. Similarly, the role of laminin in neurite lengthening and development of the nervous system as mentioned in the preceding chapter is well studied[25–27]. To quote another example, collagen I is well established as the dominant ECM type secreted by and surrounding fibroblasts[38]. Moreover, the ECM composition in fetal tissues which typically had been associated with scar-free wound healing is known to differ significantly in composition and organization compared to adult tissues[39]. In other studies, cell-ECM interaction had been reported to regulate embryonic stem cell self-renewal[40] and differentiation[41]. More recently, collagen was found to be a barrier in reprogramming of fibroblasts to induced pluripotent stem cells (iPSCs), suggesting a role of the extracellular matrix in cell reprogramming[42].

3.1.2 Tissue decellularization

The tissue specificity of ECM has been suggested to be advantageous in maintaining relevant cell phenotype and function[43–45] and a wide range of tissues have been studied in this respect. To obtain only the ECM, tissues are typically decellularized to remove their cells. This is essential since any residual cells, even if autologous in nature, can illicit an inflammatory response[46]. A variety of decellularization methods exist[47] and the method chosen varies depending on the characteristics of the specific tissue to be decellularized. Decellularization has been employed in many bioengineering applications that are highly clinically relevant. A number of clinical products are in fact decellularized tissues[47] and more are currently in clinical trails[48–50]. Allogenic and xenogenic whole organs[51,52] have also been decellularized. These decellularized organs or tissues are then essentially ECM scaffolds that can be transplanted for *in situ* remodeling and regeneration within the recipient. Successful decellularization, defined as reduction of genetic material to below threshold levels, is one key determinant of transplantation success since it can otherwise be immunogenic and [53] potentially lead to graft failure.

3.1.3 Human amnion and placenta

The human amnion and placenta are tissues that only develop during pregnancy. The amnion provides a protective environment for the fetus as it develops while the placenta is a highly innervated organ necessary for nutrient, gas and waste exchange between the maternal and fetal circulation during pregnancy. Both are no longer needed after birth. Considering that 1) supply is unlikely to be a problem, 2) both are the only healthy tissue of human origin frequently disposed of and hence readily available, 3) there are no ethical concerns related to their use and 4) both tissues are relatively "young" fetal-like tissues that had only developed post-fertilization and therefore could not be more than 10 months old, scientists often study these tissues for a wide range of potential applications. As early as 1910, the amnion has been used as skin grafts to granulating wounds[54]. Since then, it has also been used in reconstructive plastic surgery on burned and ulcerated skin[55,56], reconstruction of orofacial defects[57,58], as a barrier with low cell adhesion post-operation[59,60], in chronic wounds[61], in conjunctival reconstruction[62,63] and in cornea replacement[64,65]. More recently, there is great interest in amnion-derived stem cells for potential clinical applications due to their high plasticity[66] and low immunogenicity[67,68]. The placenta on the other hand has been traditionally used for extraction of commercially available extracellular matrix (ECM) proteins of human origin. However, these are mostly in the form of a single purified ECM protein instead of being fully representative of the complete placenta ECM. Since individual protein components of the ECM are each known for different effects, we deduce that a mixture may modulate cellular behavior differently. We were therefore interested to prepare a representative whole amnion and/or placenta ECM. In our work, we first decellularized the amnion and placenta to remove cellular proteins and leave only the ECM proteins. The ECM proteins were subsequently extracted in soluble form and used in further studies.

3.2 Materials and Methods

Decellularization of amnion and placenta Human term amnion and placenta were separated and then frozen before the placenta was processed into 3mm slices. Frozen samples were thawed and rinsed extensively with water to remove blood. Samples were then rinsed twice in 1N NaCl before decellularization with a detergent solution comprising CHAPS (8mM), EDTA (25mM) and NaCl (1mM) under gentle agitation for 2hrs at rt. This was repeated twice with samples becoming visible whiter/paler before extensive rinses in 1X PBS. This was followed by treatment with Benzonase® nuclease at 37°C overnight under gentle agitation according to manufacturer's protocol before washing with 1X PBS followed by water. Samples were further treated in a solution of peracetic acid (0.1% v/v) and ethanol (4% v/v) in water overnight before extensive washes in 1X PBS followed by ddH_2O to obtain the final decellularized tissue product.

Quantification of residual dsDNA DNA was extracted from the soluble protein solutions using the DNeasy® Blood & Tissue Kit (Qiagen) according to manufacturer's protocol. The extracted DNA was quantified using the Quant-iT™ PicoGreen® dsDNA Kit (Invitrogen) according to manufacturer's protocol. Residual dsDNA was determined and normalized to per mg of protein.

Soluble extraction of extracellular matrix proteins Decellularized samples were homogenized in urea buffer (2M) and stirred overnight at 4°C. The following day, the supernatant was collected after centrifugation and the pellet was rinsed by homogenization with fresh urea buffer. The supernatants were combined after centrifugation and dialyzed for 2hrs in 1X PBS containing chloroform (0.5% v/v) at 4°C. The dialysis solution was replaced thrice over a 24hr period with fresh 1X PBS before this non-collagenous protein fraction was collected and stored for further use. The pellet from the centrifugation was further processed with pepsin in citric acid (0.05M) under agitation overnight at 4°C before being adjusted to pH 7.5 and agitated for another 24hrs. The samples were centrifuged and pH of the supernatant was tuned to 5. NaCl was added to 1.8M and allowed to stir overnight. Samples were centrifuged, the supernatant was discarded and the pellet dissolved in 0.01N HCl to obtain the collagenous protein fraction. A layer of chloroform was added to the bottom of the tube containing the collagenous fraction before carefully extracting only the top aqueous layer after 24hrs.

Protein quantification and Western blotting Samples were quantified using the BCA protein assay kit (Pierce). 10ug of protein samples were separated on 4-15% SDS-PAGE gels, transferred to polyvinylidene difluoride membranes, blocked in 3% non-fat milk and incubated at 4°C overnight with primary antibodies (Refer to Table 3.1). Membranes were incubated with HRP-conjugated IgG secondary antibodies (Santa Cruz Biotechnologies, 1:2000) and protein bands visualized using Western Lightning Plus-Enhanced Chemiluminescence Substrate (Perkin Elmer Life & Analytical Sciences) on a digital imager (Bio-rad).

Table 3.1 Antibodies used in Western blotting

Antibody	Vendor	Catalog #	Dilution
Laminin	Millipore	AB19012	1:1000
Entactin	Millipore	MAB1886	1:1000
Collagen I	Abcam	Ab138492	1:2000
Collagen II	Abcam	Ab761	1:500
Collagen III	Abcam	Ab23445	1:1000
Decorin	Abcam	Ab151988	1:1000
PLGF	Abcam	Ab97618	1:250 (2μg/ml)
VEGF	Abcam	Ab69479	1:1000
GAPDH	Santa Cruz	32233	1:2000

Use of placenta ECM Both non-collagenous and collagenous fractions were used together. To do so, both fractions were diluted in their respective solvents to 0.2mg/ml. Plates were first coated for 1hr with the collagenous fraction at 13μg/cm^2. This was rinsed well in 1X PBS before adding the non-collagenous fraction at 7μg/cm^2 for another 1hr. Other matrix coatings used in this study included gelatin, rat tail collagen I (BD) and Matrigel® (Corning). Collagen was diluted in 0.02N acetic acid and Matrigel® in plain DMEM to 0.2mg/ml. Collagen and Matrigel® were coated at 20μg/cm^2 for a total of 2hrs at 37°C before use. Gelatin was used at 0.1% w/v at the same volume as the other three matrices.

***In vitro* cell proliferation assay** Cell viability and proliferation were respectively determined using the alamarBlue® cell viability assay and the Click-iT EdU Alexa Fluor 488 Imaging Kit (Thermo Fisher) according to manufacturer's protocol. In both assays, cells were seeded at 3000cells/cm^2 onto surfaces coated with the respective ECM proteins and allowed to adhere overnight for 16hrs before assaying.

Cell culture and differentiation media Primary fibroblasts isolated from adult rat heart were cultured in MEF medium (DMEM (Corning), 10% FBS (Hyclone) and 1% penicillin/streptomycin (GIBCO)). Cells were used exclusively at P1. In differentiation experiments, control cells were cultured in MEF medium. Adipogenic differentiation medium was composed of MEF medium supplemented with 1μM dexamethasone, 10μg/ml insulin and 0.5mM 3-isobutylmethalxanthine. Osteogenic differentiation medium was composed of MEF medium supplemented with 200μM ascorbic acid, 0.1μM dexamethasone and 10mM β-glycerophosphate.

Generation of induced pluripotent stem cells (iPSCs) Ear tissues from adult C57BL/6 mice were isolated, minced and partially digested in Liberase™ (0.025mg/ml, Roche) for 45mins at 37°C. Partially digested tissues were plated and fibroblasts were allowed to migrate out (P0). Isolated fibroblasts were expanded in MEF medium and used exclusively at P2 for all experiments. Fibroblasts were transduced with lentiviral vectors for overexpression of *Oct4*, *Sox2*, *c-Myc* and *Klf4* (OSKM) 24hrs before use in experiments. Transduced cells were cultured in MEF medium for 48 hours before switching to mESC maintenance medium (DMEM (Corning), 15% mouse ESC maintenance FBS (STEMCELL Technologies), 100 units/ml ESGRO® leukaemia inhibitory factor (Millipore), 0.1 mM β-mercaptoethanol (Sigma) and 1X MEM non-essential amino acids solution (GIBCO)) which was replaced daily throughout the experiment.

Lentiviral production and transduction Lentivirus was produced using established calcium phosphate transfection methods. Viral particles were concentrated using Lenti-X Concentrator (Clontech) according to manufacturer's protocol. Stable virus was aliquoted and stored at -80°C. Fibroblasts were plated and allowed to attach overnight before viral transduction in the presence of polybrene (8µg/ml, Sigma). Cells were incubated with virus for 24hrs before use in experiments.

Immunocytochemistry and other cell staining For immunostaining, samples were fixed in 4% paraformaldehyde, permeabilized in 0.25% Triton X-100 (Fisher) and blocked with 3% BSA (Sigma) in 1X PBS. Samples were incubated with primary antibodies (Refer to Table 3.2) overnight at 4°C followed by 1hr incubation with Alexa Fluor® 488- and/or Alexa Fluor® 546-conjugated secondary antibodies raised in donkey (Molecular Probes). Nuclei were stained with 4',6-diamino-2-phenylindole (DAPI; Invitrogen). Adipogenic differentiation was analyzed using the Oil Red O stain. Samples were fixed in 4% paraformaldehyde, rinsed well with distilled water and then equilibrated with 60% v/v isopropanol in distilled water. Fresh Oil Red O working solution was prepared by mixing 3 parts of Oil Red O stock solution (0.3% w/v Oil Red O in isopropanol) with 2 parts of distilled water and then filtered through a Whatman filter paper. Cells were stained using the Oil Red O working solution for 10mins and rinsed. Osteogenic differentiation was analyzed using the Alizarin Red S stain. Briefly samples were fixed in 4% paraformaldehyde and then rinsed well in distilled water. Cells were stained with 2% w/v Alizarin Red S solution (pH 4.2) for 2-3 mins and rinsed well. Epifluorescence or bright field images were collected using a Zeiss Axio Observer.D1.

Table 3.2 Antibodies used in immunocytochemistry

Antibody	Vendor	Catalog #	Dilution
Sca1	R&D systems	AF1226	1:100
α-SMA	Abcam	Ab32575	1:200
Calponin1	Abcam	Ab46794	1:500
Vimentin	DAKO	0725	1:1000
Nanog	Abcam	Ab70482	1:100

Preparation of placenta gels Placenta gels at a final concentration of 1mg/ml were prepared by combining 0.33mg of non-collagen extract to 0.66mg of collagen extract neutralized with 0.1N NaOH in the presence of an appropriate amount of 10X DMEM. All solutions were kept and mixed at 4°C before gelling at 37°C.

Mechanical properties of placenta gels Parallel plate rheometry was used to determine the shear modulus and gelation time of amnion and placenta gels. Samples were prepared and gelled in situ on the rheometer at 37°C under high humidity. Measurements were taken on an Anton Paar Physica MCR-301 rheometer (Anton Paar USA, Temecula, CA) using a 25 mm parallel plate geometry and analyzed using the Rheoplus software. Storage (G') and loss (G") moduli were measured at frequency of 1Hz with an amplitude gamma of 1% over 20mins at 10s intervals.

3.3 Results

3.3.1 Optimized decellularization protocol removed cells but left ECM proteins intact

Healthy term placentas weighing 450-550g were used in this study. Decellularization was initially attempted using a range of detergents of various strengths. This included CHAPS (zwitterionic), triton X-100 (non-ionic), tween 20 (non-ionic) and SDS (ionic). In selecting decellularization detergent, we were careful to use one that is sufficiently strong to remove cells but not overly strong like SDS which may disrupt ECM proteins since we were interested in isolating these ECM proteins later. Among these, we found CHAPS to be the most ideal. We initially attempted decellularization of both the amnion and placenta. Between the two, we observed that amnion was more easily decellularized since it is a thin gel-like membrane with only a single layer of cells. In contrast, the placenta required extensive detergent treatment for longer periods of time. To facilitate this process, it is crucial to pre-process the placenta into thin slices of no more than 3mm. Decellularization with CHAPs successfully removed cellular components as confirmed by the absence of GAPDH from Western blotting (Fig. 3.1c). In addition, residual dsDNA was determined to be 169ng and 284ng per mg protein extracted from amnion and placenta respectively, which is within the order of dsDNA concentration for successfully decellularized tissues[69–71]. In short, we successfully decellularized human amnion and placenta tissues with minimal loss of ECM.

3.3.2 Non-collagenous and collagenous proteins could be sequentially extracted as separate fractions from tissues

Except for Matrigel®, most commercially available ECM typically consists of one major component. In our work, we were interested in obtaining a more complete representation of the ECM present in the placenta. This may be important since the composition and interaction of the ECM proteins may influence cell behavior. Unfortunately due to their highly cross-linked nature, collagen proteins typically only solubilize after digestion in the presence of pepsin at low pH which will denature the other ECM proteins. Therefore, we adopted a two-step process in our ECM extraction where the non-collagenous proteins were first extracted before the same tissue sample was re-treated to extract collagens. In all further studies, we chose to focus on only the placenta considering its abundance relative to the amnion.

To extract the non-collagenous fraction, we tested two different extraction buffers suggested in literature[72] – 0.5M NaCl and 2M urea – and found both to be equally effective (Fig. 3.1a). Going forward, all non-collagenous proteins were extracted in a 2M urea buffer since this had a slightly shorter extraction protocol compared to NaCl. We tested for the presence of growth factors commonly found in the placenta in this non-collagen protein fraction but did not detect any. This is not surprising considering most were probably removed in the decellularization process. Collagenous proteins were solubilized by pepsin digestion followed by precipitation in NaCl before re-dissolving in 0.01N HCl. The final molarity of NaCl had previously been reported to be crucial in the precipitation process[73,74]. We tested 1.8M and 4M NaCl and observed that 1.8M was effective for precipitation of the major collagens of interest (Fig. 3.1b). Overall, we were able to sequentially extract non-collagenous and collagenous proteins from the same tissue (Fig.

3.1c) with a combined total yield of approximately 5mg protein/g of raw placenta tissue. The ratio of collagen to non-collagen proteins is approximately 2:1.

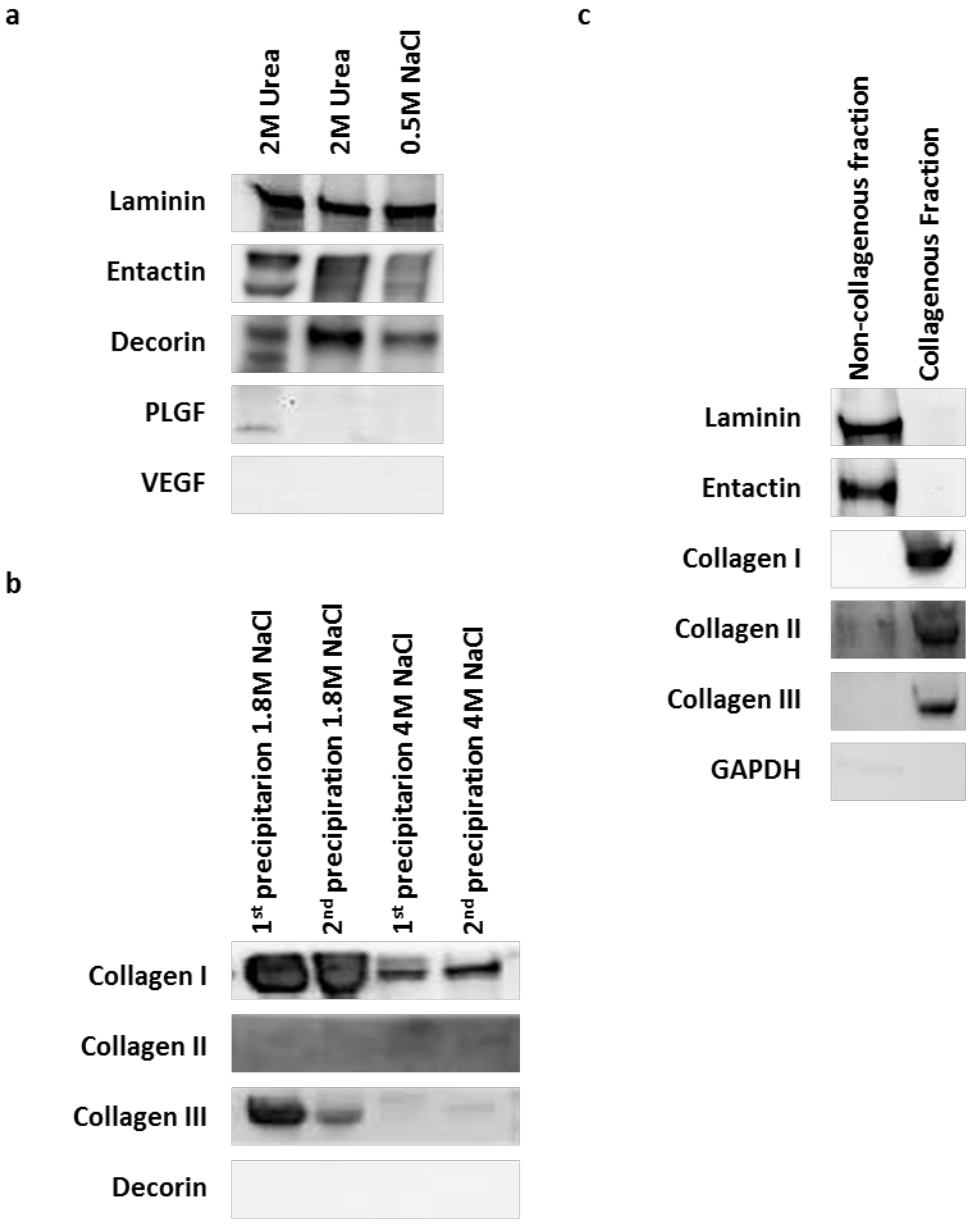

Figure 3.1 | Collagenous and non-collagenous ECM proteins can be extracted sequentially as separate fractions from human placenta. a, Optimizing extraction of non-collagenous ECM fraction using 2M urea or 0.5M NaCl. **b**, Optimizing molarity of NaCl used in precipitation of collagen from solution. **c**, Direct comparison of proteins in the non-collagenous and collagenous fraction using optimized extraction protocol.

3.3.3 *In vitro* characterization of placenta ECM on general cell properties

The chemicals and detergents utilized in the tissue decellularization and ECM extraction process are cytotoxic and detrimental to cellular health if not properly removed. To confirm that the placenta ECM do not contain any residual chemicals that may adversely affect cellular health, we compared viability and proliferation of rat cardiac fibroblasts cultured on 0.1% gelatin, collagen I or Matrigel® coated surfaces and those coated with placenta ECM. We opted to use a primary cell instead of a cell line for this study because primary cells are generally believed to be more sensitive to toxic chemicals, unlike cell lines which tend to be more robust[75]. We observed no significant difference in metabolic activity between cells cultured on placenta ECM-coated surfaces and surfaces coated with other matrices (Fig. 3.2a). Rate of cell proliferation was assayed using the Click-iT EdU Imaging kit. There was no significant difference in proliferation rates between cells cultured on the placenta ECM compared to Matrigel® or gelatin-coated surfaces (Fig. 3.2b). Cells on the collagen I surface, however, had a significantly lower rate of proliferation. Taken together, our results suggest that the placenta ECM was non-cytotoxic.

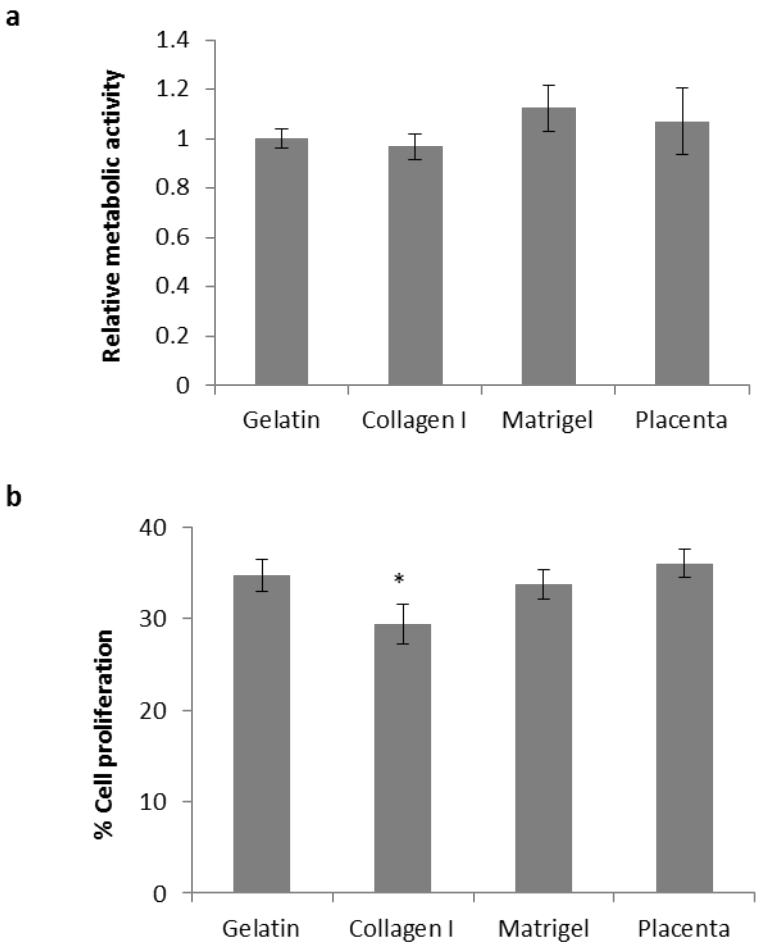

Figure 3.2 | Placenta ECM was compatible with cells and did not contain residual cytotoxic chemicals. a, Metabolic rate and **b**, proliferation rate of rat cardiac fibroblasts cultured on collagen I, Matrigel® and placenta ECM relative to gelatin. Bar graphs represent mean ± one standard deviation, n = 8 for **a** and n = 3 for **b**. Statistical significance determined by one-way ANOVA followed by Dunnett's post-hoc test, $*p \leq 0.05$ compared to placenta ECM.

To further examine if the coatings caused any differences in protein marker expression in rat cardiac fibroblasts, we performed immunostaining at 48hrs post-seeding for fibroblast markers typically expressed in this cell type. We observed similar protein expression in cells across all surface coatings (Fig. 3.3) suggesting that the placenta ECM coating did not affect cell phenotype.

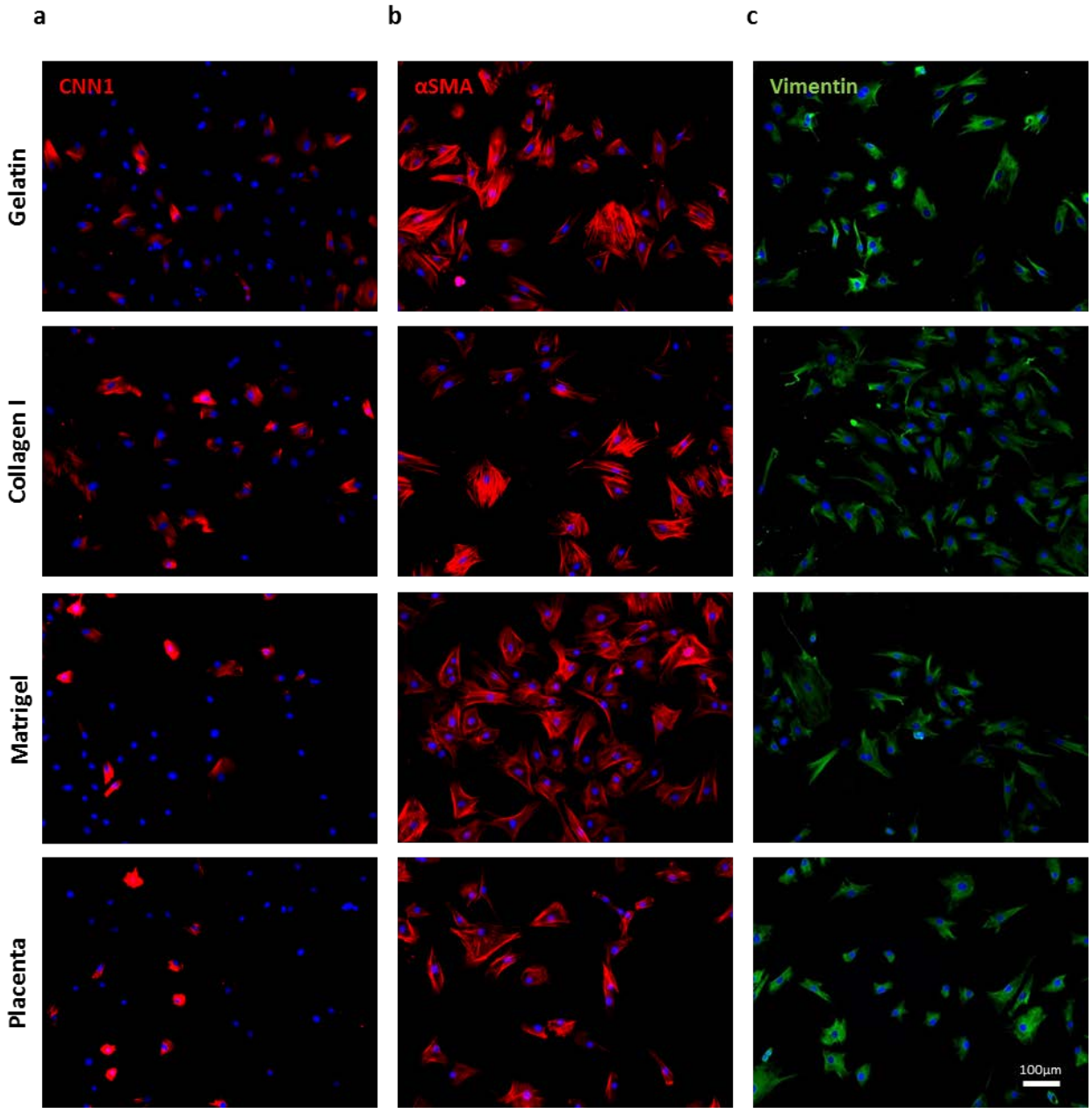

Figure 3.3 | Placenta ECM coating on culture surface did not affect cell phenotype. Immunostaining for typical fibroblast markers **a**, Calponin-1 (CNN1), **b**, alpha-smooth muscle actin (α-SMA) and **c**, vimentin in rat cardiac fibroblasts cultured on gelatin, collagen I, Matrigel® and placenta ECM (Scale bar, 100µm).

Dermal fibroblasts had previously been shown to possess multipotency, having been successfully differentiated towards various lineages using lineage-specific induction medium[76,77]. We were thus curious to investigate if this multi-lineage potential exists in cardiac fibroblasts and if so, whether the placenta ECM could preferentially skew this differentiation potential towards one lineage or another. A group of samples receiving only MEF medium was included as a control (Fig. 3.4a) and we induced differentiation towards to osteogenic and adipogenic lineages. In osteogenic differentiation cultures, we observed strong induction of the osteogenic lineage in cells cultured on collagen I-coated surfaces, as indicated by the strong staining of calcium deposits (Fig. 3.4b). The degree of osteogenic differentiation was similar on all other surface coatings tested. In adipogenic differentiation, we observed no oil droplets in cells cultured on gelatin and collagen I and only rare occurrences in the Matrigel® culture. Interestingly however, unmistakable oil droplets were found in cultures on the placenta coating as indicated by positive Oil Red staining (Fig. 3.4c). Altogether, our results show that components of the ECM may have subtle influences on the differentiation potential of cells.

3.3.4 Effects of placenta ECM on maintenance of iPSCs

Apart from examining the effects of the placenta ECM on cell differentiation, we were also curious about the effects it may have on stem cell maintenance. To investigate this, we cultured OSKM-transfected fibroblasts on surfaces coated with placenta ECM and compared them to those formed on gelatin, collagen and Matrigel® coated surfaces. We compared the degree of stem cell maintenance by quantifying the number of Nanog-positive colonies on each type of surface after 2 weeks. A representative image of a colony is shown in Fig. 3.5a. We observed no significant difference in the number of Nanog positive colonies generated across the different coatings (Fig. 3.5b).

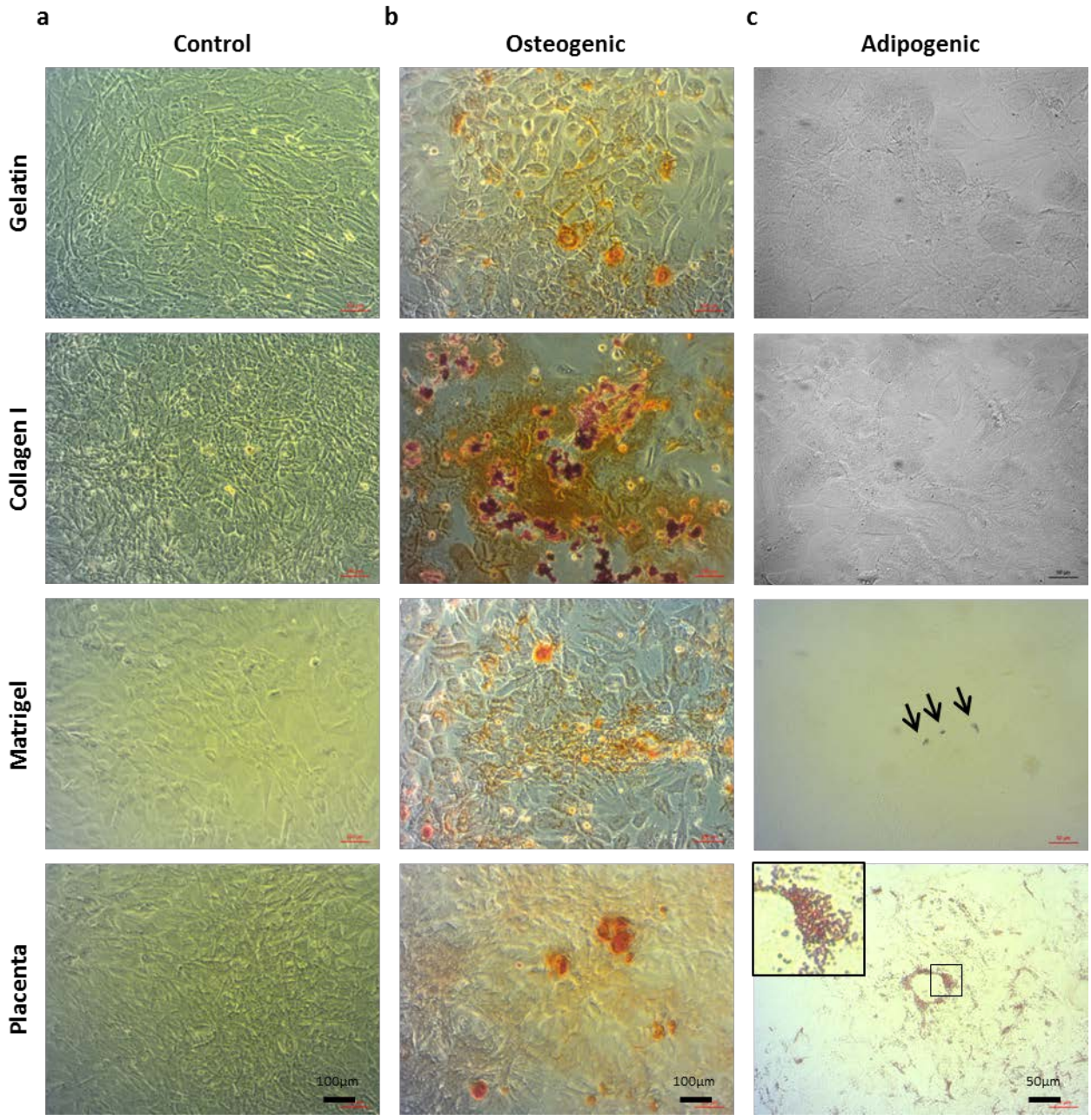

Figure 3.4 | Placenta coating on culture surface can influence differentiation potential of cells. a, Non-induced cells as a control. **b**, Culture medium-induced osteogenic differentiation of rat cardiac fibroblasts cultured on gelatin, collagen I, Matrigel® and placenta ECM (Scale bar for a and b, 100µm). **c**, Culture medium-induced adipogenic differentiation of rat cardiac fibroblasts cultured on gelatin, collagen I, Matrigel® and placenta ECM. Arrows in Matrigel image highlights rare occurrences of oil drops in this group. Insert in placenta image is a magnification of a 50 x 50µm area in center of the panel (Scale bar for c, 50µm).

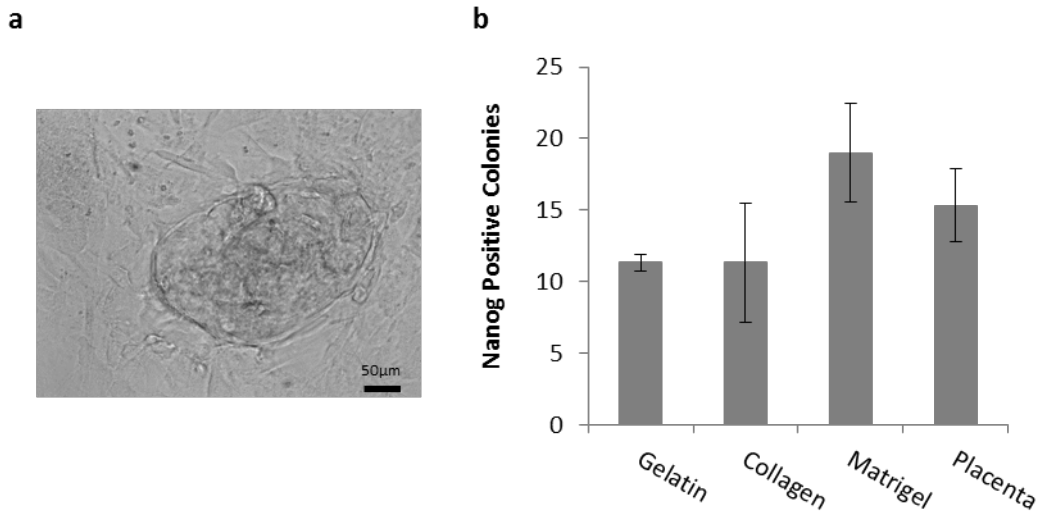

Figure 3.5 | Placenta coating on culture surface is similar to Matrigel® and may have subtle effects on maintenance of pluripotent phenotype. a, Representative image of an iPS colony generated after OSKM-transduction. **b**, Number of Nanog-positive colonies in each well of a 12 well plate coated with different protein matrices. Bar graphs represent mean ± one standard deviation, n = 3. Statistical significance determined by one-way ANOVA followed by Dunnett's post-hoc test, $*p \leq 0.05$ compared to placenta ECM.

3.3.5 Placenta ECM forms a gel similar to Matrigel® at 37°C

Matrigel® is a complex ECM commonly used as a gel in many *in vivo* laboratory applications. In fact, very encouraging results in a wide range of applications had been reported[78–80]. Unfortunately, Matrigel® is isolated from mouse tumors and being xenogenic and tumorigenic, it can never be used clinically. Since we are studying the placenta ECM as a complex matrix, we wondered if it is possible for this to replace Matrigel® in *in vivo* studies. To achieve this, the placenta ECM must first be able to gel completely at 37°C. We thus proceeded to examine the gelation properties of our placenta ECM. We observed in our preliminary studies that placenta ECM were able to form gels upon incubation overnight at 37°C. A representative image of the placenta gel (pink) is shown immersed in 1X PBS in Fig. 3.6a. To determine the gelation kinetics of the placenta ECM, we further characterized the placenta gels using a parallel plate rheometer and included Matrigel® as a comparison. The two gels had a rather different gelling profile where Matrigel® was observed to gel and reached its final storage modulus of 65 Pa almost immediately upon reaching 37°C. In contrast, the placenta gelled more slowly. We determined the shear storage modulus of the placenta gel to be approximately 59 Pa after 20mins at 37°C. This storage modulus of Matrigel® is in agreement with those previously reported in literature[81,82] obtained using rheological measurements. The time required for gelation, defined as the time when storage modulus G' is ≥ 5x loss modulus G'', was determined to be approximately 10mins (Fig. 3.6b and Table 3.3).

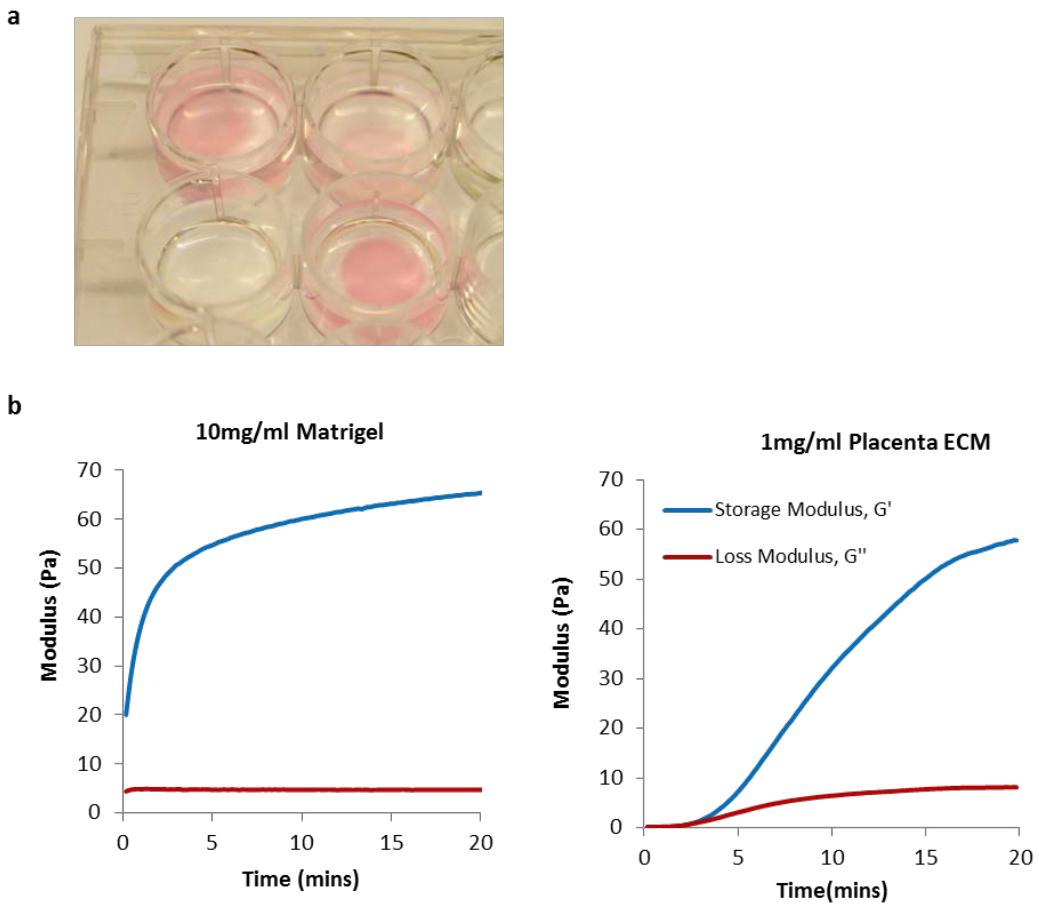

Figure 3.6 | Placenta ECM forms a gel similar to Matrigel® at 37°C. a, Representative image showing placenta gels (pink) immersed in 1X PBS (colorless). A well without gel is shown in the bottom left corner for comparison. **b**, Storage modulus, loss modulus and gelling kinetics of Matrigel® at 10mg/ml and a placenta ECM gel at 1mg/ml.

Table 3.3 Shear modulus and gelation time of Matrigel® and placenta ECM gel.

	Matrigel®	Placenta ECM
Gelling time	~Immediate	~10 mins
G' (at 1 Hz)	~65 Pa	~59 Pa

3.4 Discussion

We had initially attempted ECM extraction from both the amnion and the placenta. However, our extraction of amnion ECM yielded a lower quantity of proteins normalized to raw tissue weight compared to the placenta. This is not surprising considering that GAGs comprise a major portion of the amnion, which allows it to hold large amounts of water and gives the amnion its gel-like structure. Water is a major contributor to amnion tissue weight. In contrast, the placenta contains large amounts of connective tissues. We therefore chose to focus only on the placenta. Our observations that the placenta ECM neither adversely affect basic cellular processes such as metabolism and proliferation nor inherent cellular phenotype confirms the non-cytotoxic effects of the final product. We do believe however, that the extraction protocols can be further optimized to increase the overall protein yield. In addition, further work should also focus on attempting to preserve the growth factors from the placenta.

The strong induction of osteogenic differentiation on the collagen-coated surface is in line with known literature[83]. The effect of the placenta gel on successful adipogenic differentiation of fibroblasts under induction medium is interesting. Considering the complex composition of the placenta gel, it may contain components that facilitated the induction. This is quite unlike the other single component matrix commonly available commercially. It may be also for this same reason that the placenta gel and Matrigel® were similar in their maintenance of pluripotent cell phenotype. Although the two gels had similar storage moduli at 20mins after initiation of gelling, both had different gelling profiles with the placenta ECM needing at least 10 mins longer than Matrigel® to gel. A short gelling time is desirable since a liquid gel may quickly disperse in *in vivo* applications and become rendered useless. As such, future work should also focus on decreasing the gelling time.

Finally, we believe it will be valuable for further studies to determine the performance of the placenta gels in other applications and the extent to which placenta gel can replace Matrigel® in *in vivo* studies. If it is indeed possible, this will be particularly exciting given that it is unlikely that Matrigel® can ever be translated to clinical use regardless of how well it may perform in *in vivo* animal studies because of its sarcoma origin.

Chapter 4: Generation of a Novel Autologous Decellularized Extracellular Matrix Scaffold for Small Diameter Vascular Graft Replacement

4.1 Introduction

4.1.1 Vascular occlusion in small diameter vessels

Vascular occlusion remains the leading cause of death all over the world despite various surgical advances. The vast number of patients requiring vascular graft replacement presents a substantial clinical need, which is further compounded by an aging population. Although many viable replacements have been successfully developed for replacement of large diameter vessels (>6mm), not much have been achieved in small diameter vascular grafts (<6mm). Many patients with coronary artery disease have to undergo left ventricular assist device implantation as a bridge to heart transplantation or destination therapy, while patients with peripheral artery disease may have to suffer peripheral amputations due to lack of suitable bypass grafts. Therefore, there remains a widely recognized need for a vascular prosthesis that would be suitable for functional small-diameter vascular graft reconstruction.

4.1.2 Current clinical standards of care and challenges in small diameter graft replacement

Vascular grafts for revascularization have been widely researched in the last few decades[84]. A large variety of grafts have been studied which can be broadly categorized into decellularized natural vessels[71,85,86], collagen/other native matrix grafts[87–91] and synthetic grafts[92,93]. Synthetic grafts would have been the ideal solution since they can be pre-made in a wide range of sizes and be readily available off-the-shelf. Unfortunately, they have proven to be clinically non-feasible for small diameter applications[94] due to their tendency for thrombus formation[95] and susceptibility to infection[96,97]. Despite extensive efforts, autografts such as saphenous vein and internal mammary artery which is a method first reported back in 1949 still remain the gold-standard for treating small diameter vascular occlusive disease today. The superior performance of an autologous graft is undeniable because it does not illicit an immune response. Regrettably, a significant number of patients needing bypass surgery may not have autologous vessels of the appropriate quality or length. Even if appropriate venous tissue is available, other complications frequently lead to graft occlusion[98] and the 10-year failure rate is non-trivial[99].

4.1.3 Autologous biotubes as vascular grafts

Apart from harvesting natural vessels from patients, autologous vascular grafts can also be successfully made *in vivo* by using the tissue environment of the body (e.g. peritoneal cavity or subcutaneous) as a bioreactor. In the late 1960s, Sparks first proposed the idea of using the body's biological defense mechanism of forming fibrous capsules around foreign objects to generate a biotube around a cylindrical mandrel[100–102]. Mandrels were removed and the connective tissue biotubes were then used directly as vascular grafts in various applications. This method has since been extensively studied[103,104]. Numerous other groups have also studied variations of this in-body tissue architecture technology for clinical use with[105–107] and without[87]

anticoagulants. Unfortunately, those approaches achieved limited success in animal models and humans with low patency and high rates of complication. The fibrous tissue lining on the luminal surface of tubes was also proven to be very thrombogenic. Indeed, we also observed severe neointima hyperplasia in this kind of grafts.

4.1.4 Clinical trend - Acellular scaffolds as small diameter vascular grafts

Recent trends in academic and clinical research are shifting towards cell-free grafts and taking advantage of the regenerative capability of the body to regenerate blood vessels *in situ*[48,108–110]. In the past decade, self-assembled and scaffold-based acellular vascular grafts are entering clinical trials, with promising functional results. One product, the Cytograft is made by rolling and then fusing autologous cell sheets generated by harvesting and expanding cells from the patient[48,49]. In another study, synthetic grafts were used in combination with allogenic cells to generate an extracellular matrix (ECM) scaffold[50,71,111]. In both systems, the grafts were decellularized, implanted and allowed to regenerate *in vivo*. Decellularization has been discussed in the preceding chapter and will not be repeated here. Although the grafts in both were cell free at the point of implantation, both require extensive manipulation of cells to generate the graft, which is not only time-consuming and expensive but also faces a tougher regulatory approval process. It is therefore difficult that this approach will become standard clinical practice.

At present, the successful fabrication of an ideal autologous tissue-engineered graft for arterial revascularization remains unrealized. We develop here a novel ECM vascular graft that is both autologous and acellular for small diameter applications and does not involve any *in vitro* cellular manipulation steps. We term this the decellularized autologous vascular graft (DAVG). These acellular ECM graft scaffolds are then reimplanted into the body to allow host cells to infiltrate and remodel the graft *in vivo*. The focus of this chapter is on the early development, specifically the decellularization of the graft pre-implantation. Numerous protocols were tested, modified and optimized to obtain the most complete decellularization.

4.2 Materials and Methods

Preparation of decellularized autologous vascular grafts Teflon tubing molds were implanted into the subcutaneous pouches in the abdominal wall of Sprague-Dawley rats for 4 weeks. The implants were removed and the outer layer tubular connective tissues were detached from the Teflon tube mandrel. These autologous semi-finished vascular grafts were decellularized in a series of detergents to leave only the extracellular matrix. Briefly, samples were washed thoroughly in 1M NaCl, then treated with zwitterionic 3-[(3-Cholamidopropyl) dimethylammonio]-1-propanesulfonate (CHAPS, Sigma) detergent solution (8mM CHAPS, 1M NaCl, 25mM EDTA) for three times of 2hrs each. Decellularized common thoracic arteries underwent a further decellularization in an ionic SDS (Fisher Scientific) detergent (1.8mM Sodium dodecyl sulfate, 1M NaCl, 25mM EDTA). Both DAVGs and native arteries were then subjected to a 16 hours benzoase nuclease (Sigma) treatment (90U/ml, 50mM Tris-Cl) before being chemically conjugated with heparin. All samples were rinsed thrice with PBS and stored at 4°C for further use.

Western blotting A 2 cm length of each decellularized sample was homogenized in C-tubes (Miltenyl Biotec) on the gentle MACs dissociator (Miltenyl Biotec) with 300 uL lysis buffer (G-biosciences) supplemented with protease inhibitors (PMSF, Na_3VO_4 and leupeptin). After centrifugation, the supernatant was collected then quantified using the DC protein assay (Bio-Rad). Samples (10 ug/well) were separated by SDS-PAGE (10% gel) and transferred onto PVDF membranes. The membranes were blocked in 3% non-fat milk and incubated at 4°C overnight with primary antibodies (Table 4.1). Membranes were incubated with HRP-conjugated IgG secondary antibodies (Santa Cruz Biotechnologies, 1:2000) and protein bands were visualized using Western Lightning Plus-Enhanced Chemiluminescence Substrate (Perkin Elmer Life & Analytical Sciences) on a digital imager (Bio-Rad).

Table 4.1 Antibodies used in Western blotting

Antibody	Vendor	Catalog #	Dilution
Fibronectin	Abcam	Ab2413	1:2000
Actin	Santa Cruz	SC-1616	1:1000
α-SMA	Abcam	Ab32575	1:5000
Calponin1	Abcam	Ab46794	1:10000
FSP1	Abcam	Ab27957	1:1000
GAPDH	Abcam	Ab8245	1:2000

Quantification of residual dsDNA Decellularized samples were lyophilized in a pre-weighed Eppendorf tube. The weight of the sample was determined and recorded post-lyophilization before being homogenized in C-tubes (Miltenyl Biotec) on the gentle MACs dissociator (Miltenyl Biotec) with 300 uL 1X PBS. Sample was centrifuged and the supernatant discarded. DNA was extracted from the DAVG pellet using the DNeasy® Blood & Tissue Kit (Qiagen) according to manufacturer's protocol. The extracted DNA was quantified using the Quant-iT™ PicoGreen® dsDNA Kit (Invitrogen) according to manufacturer's protocol. Residual dsDNA was determined and normalized to per mg of dried tissue weight.

Histological Analysis Samples for histological examination were snap-frozen in optimal cutting temperature (OCT) Compound (Tissue Tek), and sectioned to 8-µm thickness. Sections were fixed in 4% paraformaldehyde. Nuclei were stained with 4',6-diamino-2-phenylindole (DAPI; Invitrogen) or H&E. Masson's trichrome staining was performed using the a kit from American MasterTech Scientific Inc according to manufacturer's protocol. Immunofluorescence images were collected with a confocal microscope (Zeiss LSM710) and bright-field images were collected on a light microscope (Zeiss).

Scanning Electron Microscopy Vascular grafts were fixed, dehydrated and critical point dried according to the established protocol. All specimens were mounted on aluminium stubs using sticky carbon taps and coated with a thin layer of Au/Pd using a Gatan ion beam coater. Images were recorded with a Hitachi TM-1000 scanning electron microscope.

4.3 Results

4.3.1 CHAPS is the optimal decellularization detergent for preparation of DAVGs

The poor patency of non-decellularized tissue engineered grafts is a known problem. Research from our lab have confirmed that the cells that were already present in the graft pre-implantation were frequently the cause of the neointima formation and that very few cells in the neointima originated from the host. Given this knowledge, we questioned if removing these cells would be a solution to the patency problem. To test our hypothesis, we generated DAVGs. A few decellularization protocols were tested, majority of which were intended to test the effects of using detergents of varying strengths, altering the time of each detergent wash and the effects of Benzonase® nuclease on the content of residual dsDNA. Western blotting was the primary method of analysis used for examining the residual presence of major cellular proteins post-decellularization.

Among the detergents tested, CHAPS and SDS were both found to be able to achieve good decellularization of DAVGs, removing most cellular proteins to below the limit of detection of conventional Western blotting. The Western blots for CHAPS decellularization are shown in Figure 4.1a. Between CHAPS and SDS, we decided on CHAPS since SDS is a much harsher anionic detergent. The minor amount of Actin still detected at this point was eventually successfully removed with further optimization of CHAPS treatment time. The omission or addition of a nuclease step to the decellularization treatment did not result in any detectable differences on Western blot.

To confirm that the decellularization protocol had also successfully removed the majority of DNA, residual dsDNA concentration in DAVG was determined by the Quant-IT™ PicoGreen® dsDNA assay. We were also curious to determine how essential it is to include a nuclease treatment step into the decellularization protocol. Thus, we compared residual concentration in DAVGs treated and not treated with Benzonase® nuclease. We found that although dsDNA had been significantly removed after CHAPS without nuclease treatment, dsDNA concentration was still lower in the treated samples. Considering that any residual DNA may potentially be immunogenic in the host post-implantation, we decided to include Benzonase® treatment in all future decellularizations. Our analysis showed DAVGs after Benzonase® nuclease to contain 0.67 ± 0.10 µg residual DNA/mg dried tissue weight, which is similar to the concentration range of decellularized products used clinically[69–71].

The gross appearance of the connective tissue tube before decellularization and after decellularization is shown in Figure 4.1b. Histological analysis comparing samples pre- and post-decellularization was further used as a visual demonstration that treatment with CHAPS left ECM proteins like collagen and elastin intact while successfully removing cells (Fig. 4.1c).

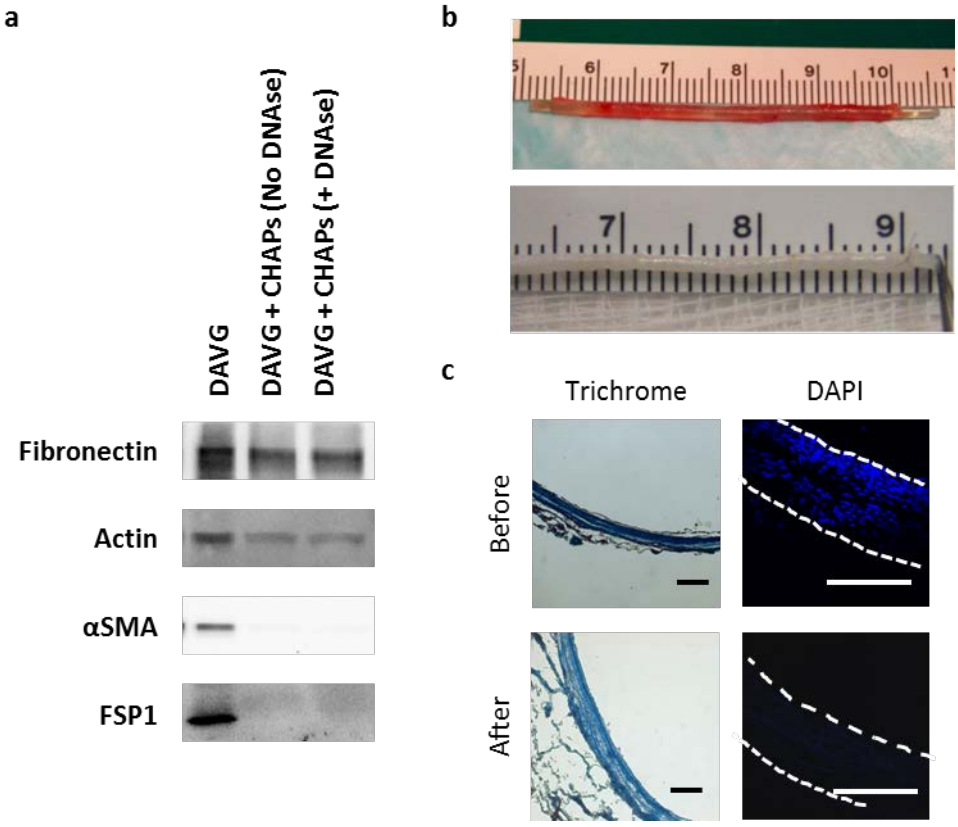

Figure 4.1 | Successful decellularization of DAVGs was obtained using CHAPS. a, Western blot for Fibronectin and key cellular proteins. Apart from actin, α-SMA and FSP1 were also tested since majority of the cells in the pre-decellularized graft are known to be fibroblasts. **b**, Gross structure of the graft. **c**, Histological staining for collagen and cell nuclei pre- and post-decellularization (scale bar, 100μm). (Credits for **c**: Xuefeng Qiu[*])

4.3.2 SDS is the optimal decellularization detergent for preparation of native aorta control

Because we intended to target the DAVGs for application in small diameter vascular graft replacement, we also prepared decellularized native thoracic aorta as a reference to compare performance of our DAVGs. This is considering that autologous vessels are still the current gold standard of care. For decellularization of native aorta, we initially attempted the same CHAPS protocol that we had optimized for DAVGs. However, we quickly realized that this was unable to achieve complete decellularization (Fig. 4.2a). We then replaced CHAPS with SDS while keeping all other steps the same, but again found it to be insufficient to completely decellularize the native thoracic aortas. After much optimization, we determined that both procedures had to be performed sequentially for successful removal of cellular components (Fig. 4.2b).

[*] Histological analysis and scanning electron microscopy were performed by Xuefeng Qiu, a CIRM clinical fellow in the lab from 2013-2015. Xuefeng is an Associate Clinical Professor from the Department of Cardiovascular Surgery at Union Hospital, Tongji Medical School, HUST in Wuhan China.

Histological staining was again used as a visual confirmation for the effectiveness of the treatment protocol (Fig. 4.2c). Concerned if the strong sequential treatment of CHAPS followed by SDS had altered the microstructure of the native aorta vessel walls, we performed scanning electron microscopy (SEM) on the gross structure and cross section and observed no obvious damage (Fig. 4.2d).

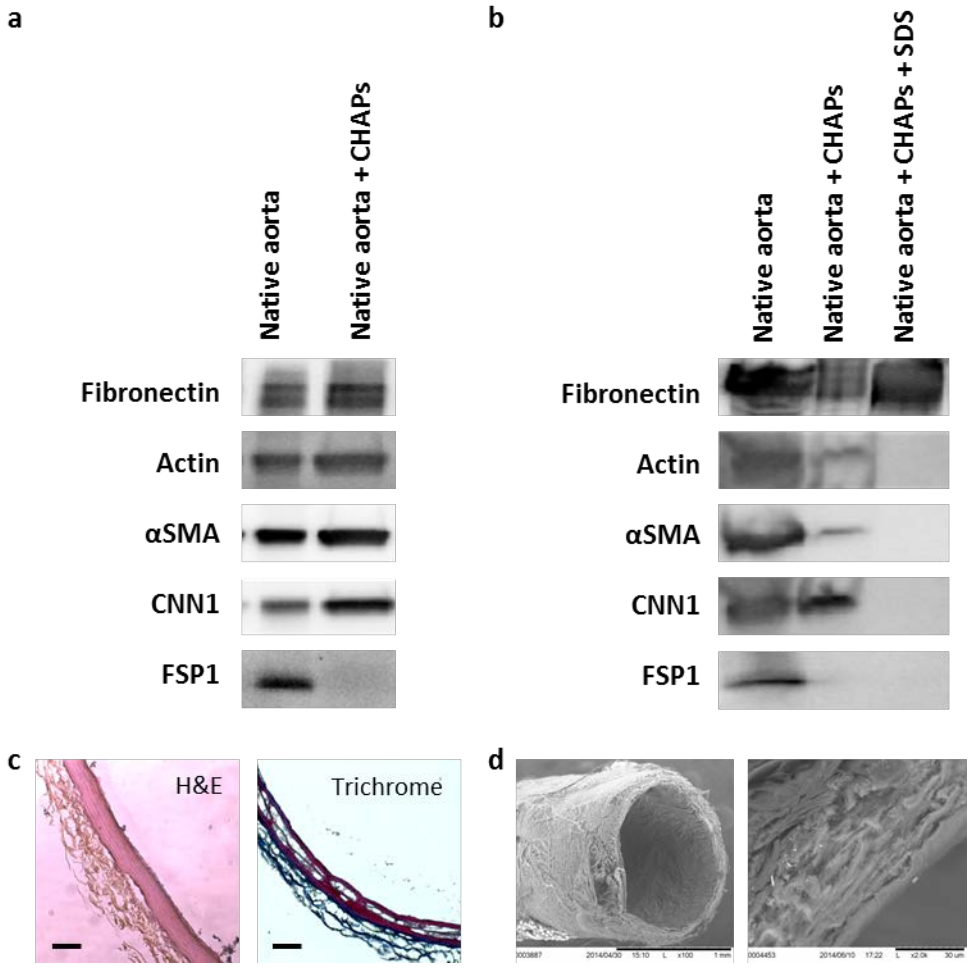

Figure 4.2 | Native aorta required sequential treatment with CHAPS and SDS for complete decellularization. a, Western blot showing presence of major cellular proteins after treatment with CHAPS indicating incomplete decellularization. **b**, Western blot demonstrating successful decellularization of native aorta after treatment with CHAPS followed by SDS. **c**, Histological staining confirming preservation of collagen and absence of cell nuclei after CHAPS + SDS (scale bar, 100μm). **d**, SEM of native aorta gross structure and cross section after CHAPS + SDS. (Credits for **c** and **d**: Xuefeng Qiu[*])

In an attempt to keep the decellularization protocol the same between DAVGs and native aorta, we applied the CHAPS + SDS protocol to DAVGs. Not surprisingly, we were able to achieve good decellularization (Fig. 4.3a) but noted from the Trichrome staining that the grafts did not appear intact. Cross section of graft walls appeared as a wavy band (Fig. 4.3b) when treated with CHAPS + SDS as opposed to a smooth band when treated with CHAPS only (Fig. 4.1c). Further investigation using SEM indicated these grafts had suffered significant structural damage (Fig. 4.3c). Moving forward, all native thoracic aorta used as controls were decellularized using a sequential CHAPS followed by SDS protocol while DAVGs were treated only with CHAPS.

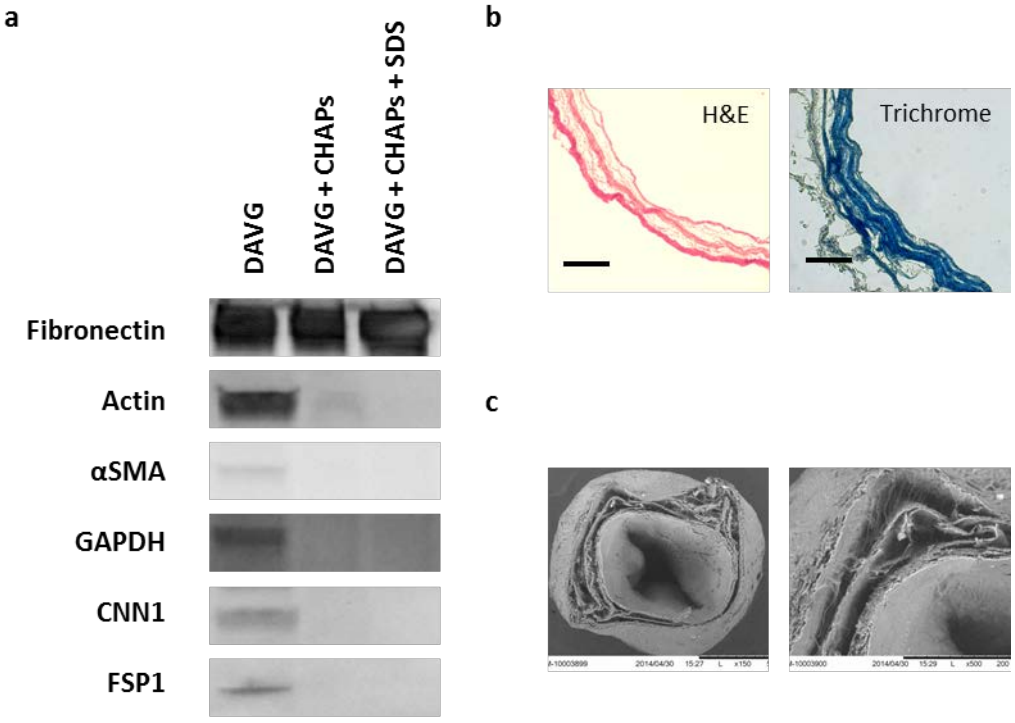

Figure 4.3 | SDS treatment was too harsh and caused structural damage to DAVGs. a, Complete decellularization of DAVGs was achieved after sequential CHAPS + SDS treatment. **b**, Histological staining showing of graft cross section (scale bar, 100μm). Notice the overall wavy appearance of the graft wall. **c**, SEM showing significant structural damage to DAVGs. (Credits for **b** and **c**: Xuefeng Qiu[*])

4.4 Discussion

We attempted multiple decellularization protocols and eventually optimized two that was able to achieve complete decellularization in our DAVG samples and native artery control. Optimization of the decellularization protocol is important since the presence of cells in the pre-implanted graft had been found to be the cause for neointima formation leading to graft failure. We wanted to obtain a protocol that was just strong enough to remove cellular components but not too harsh that it could potentially damage the samples. Of these two decellularization protocols, one uses CHAPS and the other uses CHAPS followed by SDS. Like others, we observed that CHAPS alone was insufficient to remove all cellular components from native thoracic arteries but was able to completely decellularize the DAVGs. Although it may initially seem surprising, we later found upon further investigation that ECM fibers in DAVGs had an overall looser organization which likely allowed cells and proteins to be removed more easily in contrast to the dense mass in native arteries. It may also be for this reason that the DAVGs decellularized using SDS suffered structural damage whereas DAVGs decellularized with CHAPS did not. That the DAVGs do not require SDS is also an advantage since the harsh detergent had been previously suggested to be associated with graft calcification.

Our work focused on the small diameter vascular grafts, which traditionally has been the most challenging and had highest rates of failure. Despite many limitations, autografts are still the current gold standard for small diameter grafts. We utilized the natural response of the body to form fibrous capsules around foreign objects to generate a connective tissue tube of the desired diameter. We presented here an *in vivo*-generated vascular graft that is decellularized and then autologously reimplanted back into the same animal it was generated in. The idea is truly novel in that it is a unique combination of natural ECM protein scaffold that is both autologous and acellular without extensive *in vitro* manipulation of cells. Both parameters are equally important yet previously reported grafts were either not decellularized, not of autologous origin or required extensive *in vitro* manipulation of cells. An acellular graft presents huge benefits in terms of handling, storage, low immune response and time required for regulatory approval. Importantly, a wide range of graft diameters can easily be achieved to match each specific application which decreases likelihood of graft occlusion due to size mismatch.

The *in vivo* remodeling of the graft is not the focus of this chapter but has been studied extensively in rats by others in our lab. Preliminary results demonstrate that post-remodeling DAVGs are microstructurally, mechanically and chemical-compositionally similar to the native arteries and had remarkable long term patency without any anti-platelet treatment or pre-seeded cells. This indicates DAVGs as a highly feasible idea worthy of further study. We envision this to be applied in AV shunts and peripheral artery replacements required due arteriosclerosis or other diseases. Some may argue that this method requires two surgeries and involves a long wait time for the graft to generate in the patient's body. However, the process could potentially also be performed by minimally invasive microsurgery. Besides, except in emergency cases requiring immediate treatment, the benefits of long term patency far surpass that initial time investment.

Chapter 5: Concluding Remarks and Future Directions

In classical molecular and cell biology, a cell is thought to undergo changes in response to binding of a stimulating ligand to a specific receptor. In this dissertation, however, we take a bioengineering approach and consider instead cellular responses to substrate stiffness (a biophysical factor) and ECM (a biochemical factor) surrounding them in their microenvironment. Although it is well-recognized by now that these factors do make significant contributions to directing cell fate, many unknowns still exist.

Our work in Chapter 2 filled the knowledge gap that previously existed regarding the influence of substrate stiffness on direct reprogramming. Using direct neuron reprogramming as a model system, we presented the novel finding that the intermediate stiffness is optimal for direct neuron reprogramming and further elucidated that this occurred through the modulation of cell signaling pathways. In addition, we highlighted the importance of substrate stiffness during the early phase of direct reprogramming, which potentially suggests that direct reprogramming is not a single phase process and there exists windows of opportunities during which cells may be more sensitive to their microenvironment. Importantly, our results indicate that the same biophysical factor can exert different effects on differentiation and reprogramming, which are two opposite processes. It will be interesting going forward to investigate the effects of cytoskeleton disruption and epigenetic modifications on direct reprogramming.

In Chapter 3, we isolated and characterized soluble complex ECM from human term placentas. Considering that this is isolated from a healthy, fetal-like tissue, this ECM can be tested in myocardial infarct models to assess its effects on tissue regeneration and scar formation. Further testing in other *in vivo* applications may eventually reveal the feasibility of replacing Matrigel® with potential clinical translation.

Finally, we presented in Chapter 4 the generation of a novel autologous acellular ECM scaffold for application in small diameter vascular graft replacement. The idea is truly novel in that it is a unique combination of natural ECM protein scaffold that is both autologous and acellular without extensive *in vitro* manipulation of cells. This ECM graft is currently being tested in rats and have shown very promising results in *in vivo* graft remodeling and long-term graft patency. Moving forward, it will be essential for a large animal study to better assess the likelihood of clinical success.

In summary, a detailed understanding of environmental cues and their collective effects on cell state is the key to the design of next generation biomaterials for precise cell fate control.

References

1. Bissell, M. J., Hall, H. G. & Parry, G. How does the extracellular matrix direct gene expression? *J. Theor. Biol.* **99,** 31–68 (1982).

2. Discher, D. E., Janmey, P. & Wang, Y.-L. Tissue cells feel and respond to the stiffness of their substrate. *Science (80-.).* **310,** 1139–43 (2005).

3. Pelham, R. J. & Wang, Y.-L. Cell locomotion and focal adhesions are regulated by substrate flexibility. *Proc. Natl. Acad. Sci.* **94,** 13661–13665 (1997).

4. Flanagan, L. A., Ju, Y.-E., Marg, B., Osterfield, M. & Janmey, P. A. Neurite branching on deformable substrates. *Neuroreport* **13,** 2411–2415 (2002).

5. Lo, C.-M., Wang, H.-B., Dembo, M. & Wang, Y.-L. Cell movement is guided by the rigidity of the substrate. *Biophys. J.* **79,** 144–152 (2000).

6. Wang, H., Dembo, M. & Wang, Y. L. Substrate flexibility regulates growth and apoptosis of normal but not transformed cells. *Am. J. Physiol. Cell Physiol.* **279,** C1345–1350 (2000).

7. Engler, A. J., Sen, S., Sweeney, H. L. & Discher, D. E. Matrix Elasticity Directs Stem Cell Lineage Specification. *Cell* **126,** 677–689 (2006).

8. Saha, K. *et al.* Substrate modulus directs neural stem cell behavior. *Biophys. J.* **95,** 4426–38 (2008).

9. Park, J. S. *et al.* The Effect of Matrix Stiffness on the Differentiation of Mesenchymal Stem Cells in Response to TGF-β. *Biomaterials* **32,** 3921–3930 (2011).

10. Gurdon, J. B. The Developmental Capacity of Nuclei taken from Intestinal Epithelium Cells of Feeding Tadpoles. *J. Embryol. Exp. Morphol.* **10,** 622–640 (1962).

11. Takahashi, K. & Yamanaka, S. Induction of Pluripotent Stem Cells from Mouse Embryonic and Adult Fibroblast Cultures by Defined Factors. *Cell* **126,** 663–676 (2006).

12. Davis, R. L., Weintraub, H. & Lassar, A. B. Expression of a Single Transfected cDNA Converts Fibmblasts to Myoblasts. *Cell* **51,** 987–1000 (1987).

13. Zhou, Q., Brown, J., Kanarek, A., Rajagopal, J. & Melton, D. A. In vivo reprogramming of adult pancreatic exocrine cells to β-cells. *Nature* **455,** 627–32 (2008).

14. Ieda, M. *et al.* Direct Reprogramming of Fibroblasts into Functional Cardiomyocytes by Defined Factors. *Cell* **142,** 375–386 (2010).

15. Schnerch, A. *et al.* Direct conversion of human fibroblasts to multilineage blood progenitors. *Nature* **467,** 521–526 (2010).

16. Vierbuchen, T. *et al.* Direct conversion of fibroblasts to functional neurons by defined factors. *Nature* **463,** 1035–41 (2010).

17. Pang, Z. P. *et al.* Induction of human neuronal cells by defined transcription factors. *Nature* **476,** 220–223 (2012).

18. Pfisterer, U. *et al.* Direct conversion of human fibroblasts to dopaminergic neurons. *Proc. Natl. Acad. Sci.* **108,** 10343–10348 (2011).

19. Caiazzo, M. *et al.* Direct generation of functional dopaminergic neurons from mouse and human fibroblasts. *Nature* **476,** 224–227 (2011).

20. Ladewig, J. *et al.* Small molecules enable highly efficient neuronal conversion of human fibroblasts. *Nat. Methods* **9,** 575–578 (2012).

21. Li, X. *et al.* Small-Molecule-Driven Direct Reprogramming of Mouse Fibroblasts into Functional Neurons. *Cell Stem Cell* **17,** 195–203 (2015).

22. Hu, W. *et al.* Direct Conversion of Normal and Alzheimer's Disease Human Fibroblasts into Neuronal Cells by Small Molecules. *Stem Cell* **17,** 204–212 (2015).

23. Kulangara, K. *et al.* The effect of substrate topography on direct reprogramming of fibroblasts to induced neurons. *Biomaterials* **35,** 5327–5336 (2014).

24. Tse, J. R. & Engler, A. J. Preparation of hydrogel substrates with tunable mechanical properties. *Curr. Protoc. Cell Biol.* **Unit 10.16,** 1–16 (2010).

25. Venstrom, K. A. & Reichardt, L. F. Extracellular matrix. 2: Role of extracellular matrix molecules and their receptors in the nervous system. *FASEB* **7,** 996–1003 (1993).

26. Manthorpe, M. *et al.* Laminin promotes neuritic regeneration from cultured peripheral and central neurons. *J. Cell Biol.* **97,** 1882–1890 (1983).

27. Baron-Van Evercooren, A. *et al.* Nerve growth factor, laminin, and fibronectin promote neurite growth in human fetal sensory ganglia cultures. *J. Neurosci. Res.* **8,** 179–193 (1982).

28. Lin, X., Liang, M. & Feng, X.-H. Smurf2 is a ubiquitin E3 ligase mediating proteasome-dependent degradation of Smad2 in transforming growth factor-β signaling. *J. Biol. Chem.* **275,** 36818–36822 (2000).

29. Chanda, S. *et al.* Generation of induced neuronal cells by the single reprogramming factor ASCL1. *Stem Cell Reports* **3,** 282–296 (2014).

30. Dennis, G. J. *et al.* DAVID: Database for Annotation, Visualization, and Integrated Discovery. *Genome Biol.* **4,** 3 (2003).

31. Huang, D. W., Sherman, B. T. & Lempicki, R. A. Systematic and integrative analysis of large gene lists using DAVID Bioinformatics Resources. *Nat. Protoc.* **4,** 44–57 (2009).

32. Hirai, H. & Kikyo, N. Inhibitors of suppressive histone modification promote direct reprogramming of fibroblasts to cardiomyocyte-like cells. *Cardiovasc. Res.* **102,** 188–190 (2014).

33. Sun, Y. *et al.* Hippo / YAP-mediated rigidity-dependent motor neuron differentiation of human pluripotent stem cells. *Nat. Mater.* **13,** 599–604 (2014).

34. Shou, J., Rim, P. C. & Calof, A. L. BMPs inhibit neurogenesis by a mechanism involving degradation of a transcription factor. *Nat. Neurosci.* **2,** 339–45 (1999).

35. Wapinski, O. L. *et al.* Hierarchical mechanisms for direct reprogramming of fibroblasts to neurons. *Cell* **155,** 621–635 (2013).

36. Liu, M.-L. *et al.* Small molecules enable neurogenin 2 to efficiently convert human fibroblasts into cholinergic neurons. *Nat. Commun.* **4,** (2013).

37. Bissell, M. J. & Aggeler, J. Dynamic reciprocity: how do extracellular matrix and hormones direct gene expression? *Prog. Clin. Biol. Res.* **249,** 251–262 (1987).

38. Alberts, B. *et al. Molecular Biology of the Cell*. (Garland Science, 2002). at <http://www.ncbi.nlm.nih.gov/books/NBK21054/>

39. Whitby, D. J. & Ferguson, M. W. J. The extracellular matrix of lip wounds in fetal, neonatal and adult mice. *Development* **112,** 651–668 (1991).

40. Suh, H. N. & Han, H. J. Collagen I Regulates the Self-Renewal of Mouse Embryonic Stem Cells Through α2β1 Integrin- and DDR1-Dependent Bmi-1. *J. Cell. Physiol.* **226,** 3422–3432 (2011).

41. Chen, S. S., Fitzgerald, W., Zimmerberg, J., Kleinman, H. K. & Margolis, L. Cell-Cell and Cell-Extracellular Matrix Interactions Regulate Embryonic Stem Cell Differentiation. *Stem Cells* **25,** 553–561 (2007).

42. Jiao, J. *et al.* Promoting Reprogramming by FGF2 Reveals that the Extracellular Matrix Is a Barrier for Reprogramming Fibroblasts to Pluripotency. *Stem Cells* **31,** 729–740 (2013).

43. Flynn, L. E. The use of decellularized adipose tissue to provide an inductive microenvironment for the adipogenic differentiation of human adipose-derived stem cells. *Biomaterials* **31,** 4715–4724 (2010).

44. Uygun, B. E. *et al.* Organ reengineering through development of a transplantable recellularized liver graft using decellularized liver matrix. *Nat. Med.* **16,** 814–820 (2010).

45. Sellaro, T. L. *et al.* Maintenance of Human Hepatocyte Function In Vitro by Liver-Derived Extracellular Matrix Gels. *Tissue Eng. Part A* **16,** 1075–1082 (2010).

46. Brown, B. N., Valentin, J. E., Stewart-Akers, A. M., McCabe, G. P. & Badylak, S. F. Macrophage phenotype and remodeling outcomes in response to biologic scaffolds with and without a cellular component. *Biomaterials* **30,** 1482–1491 (2009).

47. Crapo, P. M., Gilbert, T. W. & Badylak, S. F. An overview of tissue and whole organ decellularization processes. *Biomaterials* **32,** 3233–3243 (2011).

48. L'Heureux, N. *et al.* Human tissue-engineered blood vessels for adult arterial revascularization. *Nat. Med.* **12,** 361–365 (2006).

49. Mcallister, T. N. *et al.* Effectiveness of haemodialysis access with an autologous tissue-engineered vascular graft : a multicentre cohort study. *Lancet* **373,** 1440–1446 (2009).

50. Lawson, J. H. *et al.* Bioengineered human acellular vessels for dialysis access in patients with end-stage renal disease : two phase 2 single-arm trials. *Lancet* **387,** 2026–2034 (2016).

51. Ott, H. C. *et al.* Perfusion-decellularized matrix: using nature' s platform to engineer a bioartificial heart. *Nat. Med.* **14,** 213–221 (2008).

52. Petersen, T. H. *et al.* Tissue-Engineered Lungs for in Vivo Implantation. *Science (80-.).* **329,** 538–541 (2010).

53. Zheng, M. H. *et al.* Porcine Small Intestine Submucosa (SIS) Is Not an Acellular Collagenous Matrix and Contains Porcine DNA: Possible Implications in Human

Implantation. *J. Biomed. Mater. Res. Part B Appl. Biomater.* **73,** 61–67 (2005).

54. Davis, J. S. Skin transplantation with a review of 550 cases at THe Johns Hopkins Hospital. *Johns Hopkins Med. J.* **15,** 307 (1910).

55. Stern, M. The grafting of preserved amniotic membrane to burned and ulcerated surfaces, substituting skin grafts. *J. Am. Med. Assoc.* **60,** 973–974 (1913).

56. Kesting, M. R., Wolff, D. K., Hohlweg-Majert, B. & Steinstraesser, L. The role of allogenic amniotic membrane in burn treatment. *J. Burn Care Res.* **29,** 907–916 (2008).

57. Lawson, V. G. Oral cavity reconstruction using pectoralis major muscle and amnion. *Arch. Otolaryngol.* **111,** 230–233 (1985).

58. Samandari, M. H., Yaghmaei, M., Ejlali, M., Moshref, M. & Shoja, A. Use of amnion as a graft material in vestibuloplasty : A preliminary report. *Oral Surgery, Oral Med. Oral Pathol. Oral Radiol. Endod.* **97,** 574–578 (2004).

59. Young, R. L., Cota, J., Zund, G., Mason, B. A. & Wheeler, J. M. The use of an amniotic membrane graft to prevent postoperative adhesions. *Fertil. Steril.* **55,** 624–628 (1991).

60. Özgenel, G. Y. The effects of a combination of hyaluronic and amniotic membrane on the formation of peritendinous adhesions after flexor tendon surgery in chickens. *J. Bone Jt. Surg.* **86B,** 301–307 (2004).

61. Gibbons, G. W. Grafix®, a Cryopreserved Placental Membrane, for the Treatment of Chronic/Stalled Wounds. *Adv. Wound Care* **4,** 534–544 (2015).

62. de Rotth, A. Plastic repair of conjunctival defects with fetal membranes. *Arch. Opthalmology* **23,** 522–525 (1940).

63. Kim, J. C. & Tseng, S. C. Transplantation of preserved human amniotic membrane for surface reconstruction in severely damaged rabbit corneas. *Cornea* **14,** 473–484 (1995).

64. Hanada, K., Shimazaki, J., Shimmura, S. & Tsubota, K. Multilayered Amniotic Membrane Transplantation for Severe Ulceration of the Cornea and Sclera. *Am. J. Opthalmology* **131,** 324–331 (2001).

65. Solomon, A. *et al.* Amniotic Membrane Grafts for Nontraumatic Corneal Perforations , Descemetoceles , and Deep Ulcers. *Opthalmology* **109,** 694–703 (2002).

66. Parolini, O. *et al.* Concise review: isolation and characterization of cells from human term

placenta: outcome of the first international Workshop on Placenta Derived Stem Cells. *Stem Cells* **26,** 300–311 (2008).

67. Sankar, V. & Muthusamy, R. Role of human amniotic epithelial cell transplantation in spinal cord injury repair research. *Neuroscience* **118,** 11–17 (2003).

68. Bailo, M. *et al.* Engraftment potential of human amnion and chorion cells derived from term placenta. *Transplantation* **78,** 1439–1448 (2004).

69. Dahl, S. L. M., Koh, J., Prabhakar, V. & Niklason, L. E. Decellularized Native and Engineered Arterial Scaffolds for Transplantation. *Cell Transplant.* **12,** 659–666 (2003).

70. Derwin, K. A., Baker, A. R., Spragg, R. K., Leigh, D. R. & Iannotti, J. P. Commercial Extracellular Matrix Scaffolds for Rotator Cuff Tendon Repair. *J. Bone Jt. Surg.* **88A,** 2665–2672 (2006).

71. Dahl, S. L. M. *et al.* Readily Available Tissue-Engineered Vascular Grafts. *Sci. Transl. Med.* **3,** 1–11 (2011).

72. Kleinman, H. K. Preparation of Basement Membrane Components from EHS Tumors. *Curr. Protoc. Cell Biol.* 10.2.1–10.2.10 (1998).

73. Glanville, R. W., Rauter, A. & Fietzek, P. P. Isolation and Characterization of a Native Placental Basement-Membrane Collagen and Its Component α Chains. *Eur. J. Biochem.* **95,** 383–389 (1979).

74. Deyl, Z., Miksık, I. & Eckhardt, A. Preparative procedures and purity assessment of collagen proteins. *J. Chromatogr. B* **790,** 245–275 (2003).

75. Ekwall, B., Silano, V., Paganuzzi-Stammati, A. & Zucco, F. in *Short-term Toxicity Tests for Non-genotoxic Effects* 75–98 (1990).

76. Toma, J. G. *et al.* Isolation of multipotent adult stem cells from the dermis of mammalian skin. *Nat. Cell Biol.* **3,** 778–784 (2001).

77. Junker, J. P. E., Sommar, P., Skog, M., Johnson, H. & Kratz, G. Adipogenic, Chondrogenic and Osteogenic Differentiation of Clonally Derived Human Dermal Fibroblasts. *Cells Tissues Organs* **191,** 105–118 (2010).

78. Donzelli, R. *et al.* Role of extracellular matrix components in facial nerve regeneration: an experimental study. *Neurol. Res.* **28,** 794–801 (2006).

79. Patel, V. *et al.* Suspension Matrices for Improved Schwann-Cell Survival after Implantation into the Injured Rat Spinal Cord. *J. Neurotrauma* **27,** 789–801 (2010).

80. Ou, L. *et al.* Intracardiac injection of matrigel induces stem cell recruitment and improves cardiac functions in a rat myocardial infarction model. *J. Cell. Mol. Med.* **15,** 1310–1318 (2011).

81. Semler, E. J., Ranucci, C. S. & Moghe, P. V. Mechanochemical Manipulation of Hepatocyte Aggregation Can Selectively Induce or Repress Liver-Specific Function. *Biotechnol. Bioeng.* **69,** 359–369 (2000).

82. Zaman, M. H. *et al.* Migration of tumor cells in 3D matrices is governed by matrix stiffness along with cell-matrix adhesion and proteolysis. *Proc. Natl. Acad. Sci.* **103,** 10889–10894 (2006).

83. Kihara, T., Hirose, M., Oshima, A. & Ohgushi, H. Exogenous type I collagen facilitates osteogenic differentiation and acts as a substrate for mineralization of rat marrow mesenchymal stem cells in vitro. *Biochem. Biophys. Res. Commun.* **341,** 1029–1035 (2006).

84. Li, S., Sengupta, D. & Chien, S. Vascular tissue engineering : from in vitro to in situ. *WIREs Syst Biol Med* **6,** 61–76 (2014).

85. Kaushal, S. *et al.* Functional Small Diameter Neovessels using Endothelial Progenitor Cells Expanded Ex Vivo. *Nat. Med.* **7,** 1035–1040 (2001).

86. Gui, L., Muto, A., Chan, S. A., Breuer, C. K. & Niklason, L. E. Development of Decellularized Human Umbilical Arteries as Small-Diameter Vascular Grafts. *Tissue Eng. Part A* **15,** 2665–2676 (2009).

87. Ketharnathan, V. Glutaraldehyde-Tanned Ovine Collagen Conduits as Vascular Xenografts in Dogs. *Arch Surg* **115,** 967–969 (1980).

88. Ramshaw, J. A. M., Peters, D. E., Werkmeister, J. A. & Ketharnathan, V. Collagen organization in mandrel-grown vascular grafts. *J. Biomed. Mater. Res.* **23,** 649–660 (1989).

89. Cummings, C. L., Gawlitta, D., Nerem, R. M. & Stegemann, J. P. Properties of engineered vascular constructs made from collagen, fibrin, and collagen–fibrin mixtures. *Biomaterials* **25,** 3699–3706 (2004).

90. Swartz, D. D., Russell, J. A. & Andreadis, S. T. Engineering of fibrin-based functional

and implantable small-diameter blood vessels. *Am J Physiol Hear. Circ Physiol* **288,** H1451–1460 (2005).

91. Weinberg, C. B. & Bell, E. A blood vessel model constructed from collagen and cultured vascular cells. *Science (80-.).* **231,** 397–400 (1986).

92. Hashi, C. K. *et al.* Antithrombogenic property of bone marrow mesenchymal stem cells in nanofibrous vascular grafts. *Proc. Natl. Acad. Sci.* **104,** 11915–11920 (2007).

93. Yu, J. *et al.* The effect of a stromal cell-derived factor-1α /heparin coating of a biodegradable vascular graft on recruitment of both endothelial and smooth muscle progenitor cells and accelerated healing. *Biomaterials* **33,** 8062–8074 (2012).

94. Klinkert, P., Post, P. N., Breslau, P. J. & Bockel, J. H. Van. Saphenous Vein Versus PTFE for Above-Knee Femoropopliteal Bypass . A Review of the Literature. *Eur J Vasc Endovasc Surg* **27,** 357–362 (2004).

95. Greisler, H. P. Interactions at the Blood / Material Interface. *Ann Vasc Surg* **4,** 98–103 (1990).

96. Lorentzen, J. E. *et al.* No TitleVascular graft infection: an analysis of sixty-two graft infections in 2411 consecutively implanted synthetic vascular grafts. *Surgery* **98,** 81–86 (1985).

97. Antonios, V. S. *et al.* Prosthetic vascular graft infection : A risk factor analysis using a case – control study. *J. Infect.* **53,** 49–55 (2006).

98. Isenberg, B. C., Williams, C. & Tranquillo, R. T. Small-Diameter Artificial Arteries Engineered In Vitro. *Circ. Res.* **98,** 25–35 (2006).

99. Weintraub, W. S., Jones, E. L., Craver, J. M. & Guyton, R. A. Frequency of repeat coronary bypass or coronary angioplasty after coronary artery bypass surgery using saphenous venous grafts. *Am J Cardiol* **73,** 103–112 (1994).

100. Sparks, C. H. Die-Grown Reinforced Arterial Grafts: Observations on Long-term Animal Grafts and Clinical Experience. *Ann. Surg.* **172,** 787–794 (1970).

101. Sparks, C. H. Silicone Mandril Method of Femoropopliteal Artery Bypass Clinical. *Am. J. Surg.* **124,** 244–249 (1972).

102. Sparks, C. H. Silicone Mandril Method for Growing Reinforced Autogenous Femoro-Popliteal Artery Grafts in Situ. *Ann. Surg.* **177,** 293–300 (1973).

103. Campbell, J. H., Efendy, J. L. & Campbell, G. R. Novel Vascular Graft Grown Within Recipient' s Own Peritoneal Cavity. *Circ. Res.* **85,** 1173–1179 (1999).

104. Chue, W. *et al.* Dog peritoneal and pleural cavities as bioreactors to grow autologous vascular grafts. *J Vasc Surg* **39,** 859–867 (2004).

105. Satoh, S., Niu, S., Shirakata, S. & Oka, T. Development of an Autologous Connective Tissue Tube as a Small Caliber Vascular Substitute. *Trans Am Soc Artif Intern Organs* 655–660 (1988).

106. Watanabe, T., Kanda, K., Ishibashi-ueda, H., Yaku, H. & Nakayama, Y. Autologous Small-Caliber '"Biotube"' Vascular Grafts With Argatroban Loading: A Histomorphological Examination After Implantation to Rabbits. *J. Biomed. Mater. Res. Part B Appl. Biomater.* **92,** 236–242 (2010).

107. Watanabe, T. *et al.* Long-term animal implantation study of biotube-autologous small-caliber vascular graft fabricated by in-body tissue architecture. *J. Biomed. Mater. Res. Part B Appl. Biomater.* **98B,** 120–126 (2011).

108. Wu, W., Allen, R. A. & Wang, Y. Fast-degrading elastomer enables rapid remodeling of a cell-free synthetic graft into a neoartery. *Nat. Med.* **18,** 1148–1153 (2012).

109. Syedain, Z. H., Meier, L. A., Lahti, M. T., Johnson, S. L. & Tranquillo, R. T. Implantation of Completely Biological Engineered Grafts Following Decellularization into the Sheep Femoral Artery. *Tissue Eng. Part A* **20,** 1726–1734 (2014).

110. Quint, C. *et al.* Decellularized tissue-engineered blood vessel as an arterial conduit. *Proc. Natl. Acad. Sci.* **108,** 9214–9219 (2011).

111. Quint, C., Arief, M., Muto, A., Dardik, A. & Niklason, L. E. Allogeneic human tissue-engineered blood vessel. *J. Vasc. Surg.* **55,** 790–798 (2012).